https://doi.org/10.5194/egusphere-2023-1386
Preprint. Discussion started: 11 July 2023

Sea ice loss translates into major shifts in the carbonate environmental conditions in Arctic Shelf Sea

Claudine Hauri[1], Brita Irving[1], Sam Dupont[2,3], Remi Pages[1], Donna Hauser[1], and Seth Danielson[4]

[1] International Arctic Research Center, University of Alaska Fairbanks, Fairbanks, AK 99775, USA
[2] Department of Biological and Environmental Sciences, University of Gothenburg, Fiskebäckskil 45178, Sweden
[3] Radioecology Laboratory International Atomic Energy Agency (IAEA), Marine Laboratories, Principality of Monaco
[4] College of Fisheries and Ocean Science, University of Alaska Fairbanks, Fairbanks, AK 99775, USA

Correspondence email: chauri@alaska.edu

https://doi.org/10.5194/egusphere-2023-1386
Preprint. Discussion started: 11 July 2023

Abstract

Healthy Arctic marine ecosystems are essential to the food security and sovereignty, culture and wellbeing of Indigenous Peoples in the Arctic. At the same time, Arctic marine ecosystems are highly susceptible to impacts of climate change and ocean acidification. While increasing ocean and air temperatures and melting sea ice act as direct stressors on the ecosystem, they also indirectly enhance ocean acidification, accelerating the associated changes in the inorganic carbon system. Yet, much is to be learned about the current state and variability of the inorganic carbon system in remote places. Here, we present pH and pCO_2 time-series (2016-2020) from the Chukchi Ecosystem Observatory. The subsurface observatory is located in the midst of a biological hotspot with high primary productivity and a rich benthic food web that support coastal Iñupiat, whales, ice seals, walrus (*Odobenus rosmarus*), and Arctic cod (*Boreogadus saida*). Our observations suggest that near-bottom waters (33 m depth, 13 m above the seafloor) are a high carbon dioxide and low pH and aragonite saturation state environment in summer and fall, when organic material from the highly productive summer remineralizes. During this time, the aragonite saturation state can be as low as 0.4, triggering free $CaCO_3$ dissolution. During the sea ice covered winter period, pH was < 8 and aragonite remained undersaturated under the sea ice. There are only two short seasonal periods with relatively higher pH and Ω_{arag}, which we term ocean acidification relaxation events. In spring, high primary production from sea ice algae and phytoplankton blooms and ikaite dissolution lead to spikes in pH (pH > 8) and aragonite oversaturation. In late fall, strong wind driven mixing events that bring CO_2 depleted surface water to the shelf also lead to events with elevated pH and Ω_{arag}. Given the recent observations of high rates of ocean acidification, and sudden and dramatic shift of the physical, biogeochemical, and ecosystem conditions in the Chukchi Sea, it is possible that the observed extreme conditions at the Chukchi Ecosystem Observatory are significantly deviating from the carbonate conditions to which many species are adapted and may have negative impacts on the ecosystem.

1. Introduction

The quickly changing Arctic Ocean has climatic, societal, and geopolitical implications for the peoples of the Arctic and beyond (Huntington et al., 2022). Arctic Indigenous Peoples are at the forefront of this change and their food security, food sovereignty, culture, and ways of life depend on healthy Arctic marine ecosystems (ICC, 2015). The Arctic is warming at a rate that is

https://doi.org/10.5194/egusphere-2023-1386
Preprint. Discussion started: 11 July 2023

up to four times that of the rest of the globe (Serreze and Barry, 2011; Serreze and Francis, 2006; Rantanen et al., 2022). This phenomenon, called Arctic Amplification, is observed in air and sea temperatures, has accelerated in recent years, and is expected to continue in the future (Rantanen et al., 2022; Shu et al., 2022). Warming exerts a toll on sea ice extent, ice thickness, and the duration of seasonal sea ice cover: ice is forming later in fall and retreating earlier in spring, thereby increasing the length of the open water period (Stroeve et al., 2011; Serreze et al., 2016; Wood et al., 2015; Stroeve et al., 2014). The lowest Arctic wide minimum sea ice extents were recorded during last 16 years of the 44 year-long satellite time-series (National Snow and Ice Data Center).

At the same time, the Arctic Ocean is vulnerable to ocean acidification. Although oceanic uptake of anthropogenic CO_2 increases oceanic CO_2 and decreases pH and calcium carbonate ($CaCO_3$) saturation states of calcite (Ω_{calc}) and aragonite (Ω_{arag}) globally, climate induced changes to riverine input, temperature, sea ice, and circulation are accelerating the rate of ocean acidification in the Arctic Ocean like nowhere else in the world (Woosley and Millero, 2020; Qi et al., 2022a; Yamamoto-Kawai et al., 2009; Orr et al., 2022; Semiletov et al., 2016; Qi et al., 2017). Recent observational studies propose that freshening of the Arctic Ocean as a result of increased riverine input may play an even greater role in acidifying the Arctic Ocean than the uptake of anthropogenic CO_2 (Woosley and Millero, 2020; Semiletov et al., 2016). In addition, the cold Arctic waters have naturally low concentrations of carbonate ions (CO_3^{2-}) and are therefore closer to aragonite undersaturation (Ω_{arag} =1) than more temperate waters (Orr, 2011; Sarmiento and Gruber, 2006), which leads to the chemical dissolution of free aragonitic CaCO3 structures (Bednarsek et al., 2021). Because of the naturally low concentrations of CO32-, such high latitude waters have a lower capacity to take up anthropogenic CO2 and buffer these changes (Orr, 2011). As a result, concentrations of H^+ increase and pH (= -log (H^+)) decreases faster in the Arctic than in the tropics, for example.

In the Pacific Arctic, the Chukchi shelf waters have warmed by 0.45 ^oC $decade^{-1}$ since 1990, triple the rate since the beginning of the data record in 1922 (Danielson et al., 2020). Direct observations of the inorganic carbon dynamics of the Chukchi Sea are mostly limited to June through November because of the region's remoteness and accessibility during sea ice covered months. Summertime profiles across the Chukchi Sea show steep vertical gradients in inorganic carbon chemistry (Bates, 2015; Bates et al., 2009; Pipko et al., 2002; Mathis and Questel, 2013).

https://doi.org/10.5194/egusphere-2023-1386
Preprint. Discussion started: 11 July 2023

Surface waters are CO2-deplete as a result of high primary production after sea ice retreat, leading to aragonite supersaturated conditions, with Ωarag > 2 (Bates, 2015; Bates et al., 2009). In areas with sea ice melt or riverine freshwater influence, Ωarag tends to be lower and at times undersaturated (Bates et al., 2009; Yamamoto-Kawai et al., 2009). At the same time, pCO2 values near the seafloor are around 1000 µatm as a result of remineralization of organic matter, leading to summertime aragonite undersaturation (Mathis and Questel, 2013; Pipko et al., 2002; Bates, 2015). Between September and November, continuous measurements from within a few meters of the surface suggest a mosaic of pCO2 levels between ~ 200 to 600 µatm, likely due to patchy wind-induced mixing, entraining high-CO2 waters from the bottom to the surface (Hauri et al., 2013). Yamamoto-Kawai et al. (2016) used mooring observations of S, T, and apparent oxygen utilization to estimate dissolved inorganic carbon (DIC), total alkalinity (TA), and Ω_{arag} in bottom waters at their mooring site in the Hope Valley to give first insights into year round variability of the inorganic carbon system. They found slightly less intense aragonite undersaturation in spring and winter compared to summer, with a net undersaturation duration of 7.5-8.5 months per year.

The CEO is situated in a benthic hotspot where high primary production supports rich and interconnected benthic and pelagic food webs (Grebmeier et al., 2015; Moore et al., 2000). The benthos is dominated by calcifying bivalves, polychaetes, amphipods, sipunculids, echinoderms and snow crabs (Grebmeier et al., 2015; Blanchard et al., 2013). Bearded seals (*Erignathus barbatus*), walrus (*Odobenus rosmarus divergens*), gray whale (Eschrichtius robustus), and seabirds feed on these benthic calcifiers during the open water season (Kuletz et al., 2015; Jay et al., 2012; Moore et al., 2022). Prolonged open-water seasons during periods of high solar irradiance, in combination with an influx of new nutrients and wind mixing, are likely enhancing primary and secondary production as well as advection of zooplankton (Lewis et al., 2020; Arrigo and van Dijken, 2015; Wood et al., 2015). These physical processes in turn fuel keystone consumers such as Arctic cod (*Boreogadus saida*) and upper trophic level ringed seals (*Phoca hispida*), beluga (*Delphinapterus leucas*) and bowhead whales (*Balaena mysticetus*) as well as predatory polar bears (*Ursus arctos*) and Inuit who rely on the marine ecosystem for traditional and customary harvesting (Huntington et al., 2020).

Perturbation of the seawater carbonate system associated with ocean acidification and climate change can have significant physiological and ecological consequences for marine

https://doi.org/10.5194/egusphere-2023-1386
Preprint. Discussion started: 11 July 2023

species and ecosystems (IPCC 2022). All parameters of the carbonate system (pH, concentrations of pCO_2, HCO_3^-, CO_3^{--}) have the potential to affect the physiology of marine organisms while a change in Ω can lead to the dissolution of unprotected or "free" $CaCO_3$ structures. Recent work has highlighted the importance of local adaptation to the present environmental variability as a key factor driving species sensitivity to ocean acidification (Vargas et al., 2017, 2022). As the carbonate chemistry conditions and variability vary enormously between regions, marine organisms are naturally exposed to different selective pressures and can evolve different strategies to cope with low pH or Ω, or high pCO_2. For example, the deep-sea mussel *Bathymodiolus brevior* living around vents at 1600m depths is capable of precipitating calcium carbonate at pH ranging between 5.36 and 7.30 and highly undersaturated waters (Tunnicliffe et al., 2009). The response to changes in the carbonate chemistry is also modulated by other environmental drivers such as temperature or food availability (IPCC 2022). As ocean acidification imposes extra energy costs to most marine organisms, its effects can be amplified under food limitations (e.g. Thomsen et al., 2013). As a consequence, no absolute or single threshold is expected for ocean acidification (e.g. Bednaršek et al., 2021) and a pre-requisite to assessing the impact on any biota is the monitoring at a short temporal scale to characterize the present environmental niche. When it comes to future impacts, the more intense and faster the changes associated with ocean acidification, the more negative the biological impact is expected (Vargas et al. 2017, 2022). Arctic marine waters that are experiencing widespread and rapid ocean acidification are then highly likely to undergo severe negative ecosystem impacts (AMAP 2018).

Here, we present satellite sea ice coverage data and four years of nearly continuous salinity, temperature, and partial pressure of carbon dioxide (pCO_2) data, accompanied by pH, nitrate (NO_3), dissolved oxygen (O_2), and chlorophyll fluorescence data for some of the time (Table 1, Figure 2 a-h). These data allow us to determine the seasonal and interannual variability and controls of the inorganic carbon system in the Chukchi Sea between 2016 and 2020 and characterize the chemical conditions experienced by organisms.

2. Materials and Methods

2.1 The Chukchi Ecosystem Observatory

https://doi.org/10.5194/egusphere-2023-1386
Preprint. Discussion started: 11 July 2023

The Chukchi Ecosystem Observatory (CEO) is located amidst a biological hotspot near the southern tip of Hanna Shoal in the northeastern Chukchi Sea (71°35.976' N, 161°31.621' W, Figure 1, Hauri et al., 2018). The Chukchi Sea is a shallow shelf sea with maximum depths < 50 m. It is largely a unidirectional system with Pacific origin water entering the Chukchi Sea through the Bering Strait and advecting north into the Arctic Ocean.

The observatory consists of two moorings that sample year-round, equipped with a variety of sensors that measure sea ice cover and thickness (Sandy et al., 2022), light, currents, waves, salinity, temperature, concentrations of dissolved oxygen, nitrate, and particulate matter, pH, pCO_2, chlorophyll fluorescence , zooplankton abundance and vertical migration (Lalande et al., 2021, 2020), the presence of Arctic cod and zooplankton (Gonzalez et al., 2021), and the vocalizations of marine mammals. During some years, the observatory included a third mooring, an experimental "freeze-up detection mooring", which transmitted real-time data of conductivity and temperature throughout the water column until sea ice formation. The primary moorings stretch from the seafloor at 46 m to about 33 m depth, designed to avoid collisions with ice keels. A description of the CEO and a complete list of sensors deployed at the site can be found in (Hauri et al., 2018). For this study we focus on the inorganic carbon system and its controlling mechanisms (Figure 2).

2.2 pCO_2

We used a CONTROS HydroC CO_2 sensor (4H-Jena Engineering GmbH, Kiel, Germany) to measure pCO_2. The Contros HydroC CO_2 sensor was outfitted with a pump (SBE 5M, Sea-Bird Electronics) that flushes ambient seawater against a thin semi permeable membrane, which serves as equilibrator for dissolved CO_2 between the ambient seawater and the headspace of the sensor. Technical details about the sensor and its performance are described in Fietzek et al., (2014), who estimated sensor accuracy to be better than 1% with postprocessing.

A HydroC CO_2 sensor has been deployed at the CEO site since 2016. In all deployments, except 2016, HydroC CO_2 sensors were post-calibrated. The lack of post-calibration in 2016 is not expected to negatively affect data quality because a battery failure resulted in the sensor only returning data for 3 months (August through November). Five samples were collected in a burst fashion every 12 or 24 hours depending on deployment year (Table 1). Average pCO_2 values are reported as the mean of the measure interval (Table 1) with standard uncertainty calculated

https://doi.org/10.5194/egusphere-2023-1386
Preprint. Discussion started: 11 July 2023

following best practices (Orr et al., 2018) by adding in quadrature the random component of the uncertainty (standard deviation of the mean) and the systematic components (sensor accuracy and estimated error of the regression during calibration). The relative uncertainty of pCO_2 met the weather data quality goal, defined as 2.5 % by the Global Ocean Acidification Observing Network (GOA-ON, Newton et al., 2015), more than 96 % of the time.

HydroC CO_2 data were processed using Jupyter notebook scripts developed by 4H-Jena Engineering GmbH using pre- and post-calibration coefficients interpolated with any change in the zero signal reference over the deployment (Fietzek et al., 2014). Further processing using in-house MATLAB scripts included removal of outliers, calculation of the average pCO_2, and calculation of uncertainty estimates for each measurement interval.

2.3 pH

A SeapHOx sensor (Satlantic SeaFET™ V1pH sensor integrated with Sea-Bird Electronics SBE 37-SMP-ODO) was used to concurrently measure pH, salinity, temperature, pressure, and oxygen (Martz et al., 2010). A SeapHOx was deployed at CEO in 2016, 2017, and 2018. No SeapHOx was deployed in 2019 or 2020 due to supply chain delays and instrument communication issues at sea. Unfortunately, pH data from the 2016 and 2018 SeapHOx deployment were unusable due to high levels of noise in both the internal and external electrodes. The SBE37-SMP-ODO did not record any CTD or oxygen data during the 2016 deployment and only recorded CTD and oxygen data between August and November 3 in 2018 due to battery failure. In short, we only collected usable pH data between August 2017 and August 2018.

pH data were excluded during a 14-day conditioning period after the deployment and were processed with post-calibration corrected temperature and salinity from the SBE37 following (Bresnahan et al., 2014) using voltage from the external electrode, and pH_{ext} from an extended period of low variability (18 February 2018). Despite the availability of discrete data from one calibration cast (Cross et al., 2020a; Table 2, Figure 4, Figure S1), pH_{ext} was used as the single calibration point for a variety of reasons; 1) high variability of pH_{SeaFET} (0.0581 pH units) straddling a 12 hour window around when the discrete sample was collected, 2) high temporal and spatial variability often seen in the Chukchi Sea, and 3) the discrete pH sample was within the published SeaFET accuracy of 0.05 (Table 2, Figure S1). pH values are reported as the mean

https://doi.org/10.5194/egusphere-2023-1386
Preprint. Discussion started: 11 July 2023

of the measurement interval (Table 1) and standard uncertainty was calculated following best practices (Orr et al., 2018) by adding in quadrature the standard deviation of the average (random), and the SeaFET accuracy (systematic). Data handling and processing was done using in-house MATLAB scripts.

2.4 Nitrate

NO_3 measurements were from a Submersible Ultraviolet Nitrate Analyzer (SUNA) V2 by Sea-Bird Scientific. The SUNA is an *in situ* ultraviolet spectrophotometer designed to measure the concentration of nitrate ions in water. SUNA V2 data were processed using a publicly available toolbox (Hennon et al., 2022; Irving, 2021) with QA/QC steps that included thermal and salinity corrections (Sakamoto et al., 2009), assessment of spectra and outlier removal based on spectral counts (Mordy et al., 2020), and concentration adjustments (absolute offset and linear drift) based on pre-deployment and post-recovery reference measurements of zero concentration (DI) water and a nitrate standard and, when available, nutrient samples taken from Niskin bottles near the mooring site (e.g. Daniel et al., 2020).

2.5 CTD and Oxygen

Two CTDs were deployed on the CEO-2 morning near the HydroC CO_2 depth. A pumped Sea-Bird SeaCAT (SBE16) with ancillary sensors (oxygen SBE43, fluorometer, PAR) has been deployed since 2014. The other CTD was a pumped Sea-Bird MicroCAT (SBE37-SMP-ODO), with an integrated optical dissolved oxygen sensor (SBE63; Figure S2), integrated within the SeapHOx instrument that was deployed in fall 2016, 2017, and 2018, but only returned CTD and oxygen data from August 2017 through November 2018 as discussed in Section 2.3. Density and practical salinity were calculated using the TEOS-10 GSW Oceanographic Toolbox (McDougall & Baker, 2011). Oxygen was converted from ml/l to umol/kg following Bittig et al., (2018). Data processing of 2017-2018 SBE37-SMP-ODO included temperature and conductivity correction using pre- and post-calibration data following Sea-Bird Application Note 31 and oxygen correction using pre- and post-calibration data following Sea-Bird Module 28.

A pumped SBE43 was deployed at CEO-2 with the SBE16 during the 2015-2016, 2017-2018, and 2019-2020 deployments but is not discussed further because differences between the SBE43 and SBE63 of approximately 145 to 265 umol/kg were observed over the 2017-2018

https://doi.org/10.5194/egusphere-2023-1386
Preprint. Discussion started: 11 July 2023

deployment, and both moored sensors had varying offsets compared to nearby casts (Figure S2). Therefore, only relative oxygen values from the pumped SBE63 are discussed in this paper.

The freeze-up detection mooring consisted of four Sea-Bird SBE 37 inductive modem CTD sensors that transmitted in real time hourly temperature, salinity and pressure data via the surface float from four subsurface depths (8, 20, 30, and 40 m, Hauri et al., 2018).

2.6 Development and evaluation of empirical relationship to estimate pH

Empirical relationships for estimating water column pH have been developed for regions spanning Southern, tropical, temperate and Arctic biomes, using a variety of commonly measured parameters (e.g. pH(S, T, NO_3, O_2, Si) Carter et al., 2018; pH(O_2,T,S) Li et al., 2016; pH(θ,O_2) Watanabe et al., 2020; pH(NO_3, T, S, P) and pH(O_2, T, S, P) Williams et al., 2016; pH(O_2, T) Alin et al., 2012; pH(O_2, T) and pH(NO_3, T) Juranek et al., 2009). Given the tight coupling between the concentration of hydrogen ion and concentration of CO_2 solution, an empirical relationship for estimating surface pH from pCO_2 was developed by the National Academies of Sciences, Engineering and Medicine (2017) appendix F. Licker et al., (2019) used this empirical relationship to calculate the global average surface ocean pH and found it represented the relationship for surface water temperatures spanning 5°C to 45°C. Here we take a similar approach but extend it to water column pH in our cold region using temperature (T) and salinity (S) as additional proxy parameters (Equation 1).

$$pH^{est} = \alpha_0 + \alpha_1 log\,(pCO_2) + \alpha_2 T + \alpha_3 S \quad (1)$$

Where pH^{est} is the estimated proxy value of water column pH, pCO_2 is from the HydroC, and T and S are from the SBE16, and all α (α0 = 10.4660, α1= -0.4088, α2 = 0.0013, α3 = -0.0001) terms are model-estimated coefficients determined using MATLAB's multiple linear regression algorithm *regress.m*. After interpolating pH_{SeaFET} (Figure 3, gray dots) to the pCO_2 data timestamps (Figure 3, black dots), the algorithm was trained over a 180-day time period (15/9/2017-14/3/2018) (Figure 3, shaded area). An uncertainty estimate for pH^{est} of 0.0525 (Figure S1, blue shading) was determined by adding in quadrature the RMSE (the uncertainty in estimation) over the entire pH_{SeaFET} time series and the published accuracy of the SeaFET.

Estimated pH (Figure 3, red line) represents pH_{SeaFET} reasonably well across the whole time series (r^2 = 0.9598, RMSE = 0.0161, $p<0.0001$, Figure 4), over the training period (r^2 = 0.9321, Figure 4d shaded area), and outside of the training period (r^2 = 0.9666). The observed high

https://doi.org/10.5194/egusphere-2023-1386
Preprint. Discussion started: 11 July 2023

frequency spikes in pH_{SeaFET} were not captured by the HydroC pCO_2 sensor and as a result are not reproduced in the pH^{est} time series. Throughout the pH_{SeaFET} time series pH^{est} overestimates pH_{SeaFET} by a mean of 0.0008 and median of 0.0039. Discrete values were used to evaluate the algorithm at the CEO site (Table 2) and found to be within the pH^{est} uncertainty (Figure S1).

The algorithm was further evaluated using discrete data collected from the Bering Sea to the Arctic Ocean on four research cruises in 2020, 2019, 2018, and 2017 (Figure 5d; Monacci et al., 2022; Cross et al., 2021; 2020a; 2020b) and showed good agreement with the *in situ* samples (Figure 5). Samples collected below 500 dbar or flagged as questionable or bad were excluded from this analysis. pH^{disc}_{calc} and $pCO_2{}^{disc}_{calc}$ were calculated from 1275 discrete samples analyzed for TA, DIC, silicate, phosphate, and ammonium (except when silicate, phosphate, and ammonium were assumed zero for the 327 samples from SKQ202014S) using CO2SYSv3 (Sharp et al., 2023; Section 2.3 for details). pH^{disc}_{est} was calculated using Equation 1 and was fit to pH^{disc}_{calc} using a linear regression model ($R^2 = 0.9975$, RMSE = 0.0078, p-value < 0.0001; Figure 5a). Mean differences between pH^{disc}_{est} and pH^{disc}_{calc} were zero, with a median of -0.0022, with largest anomalies observed at lower salinities (Figure 5c). Observed absolute differences between pH^{disc}_{est} and pH^{disc}_{calc} over the salinity range observed at the CEO site (30.87 to 33.93) fall within the weather data quality goal (Newton et al., 2015) 98.7% of the time with maximum absolute differences < 0.03. An estimate for the uncertainty of the algorithm (Equation 1) of 0.0154 was determined by adding in quadrature the mean combined standard uncertainty (u_c) for pH^{disc}_{calc} (0.0133; Orr et al., 2018) and the regression RMSE.

2.7 Carbonate system calculations

Moored data were collected at different sample intervals (Table 1) and were linearly interpolated to the HydroC CO_2 timestamp to enable further calculations. TA, DIC, and Ω_{arag} (Figure 2 i-k) were based on data from the HydroC CO_2, pH^{est} and S, T, and pressure (P) from the SBE16. Nutrient concentrations (Si, PO_4, NH_4, H_2S) were assumed to be zero. pH^{est} was used in lieu of pH_{SeaFET} to allow for calculations over the whole pCO_2 record and due to erroneously large variability of DIC and TA when pH_{SeaFET} was used as an input parameter (Raimondi et al., 2019; Cullison-Gray et al., 2011). The pH-pCO_2 input pair leads to large calculated errors in DIC and TA (Raimondi et al., 2019; Cullison-Gray et al., 2011) due to strong covariance between the two parameters (both temperature and pressure dependent). Cullison-Gray et al.,

https://doi.org/10.5194/egusphere-2023-1386
Preprint. Discussion started: 11 July 2023

(2011) attributed unreasonably large short-term variability in calculated TA and DIC to temporal or spatial measurement mismatches between input pH and pCO_2 parameters and found that appropriate filtering alleviated noise spikes. By using pH^{est}, which by the nature of its definition is well correlated to pCO_2, we are eliminating some of these spurious noise spikes. We show Ω_{arag} calculated from pH_{SeaFET}-pCO_2 (Figure 2k, gray line) because it is less sensitive to calculated errors as it accounts for a small portion of the total CO_2 in seawater (Cullison-Gray et al., 2011). pH is reported in total scale for the entirety of this paper.

All inorganic carbon parameters were calculated using CO2SYSv3 ; Lewis and Wallace, 1998) with dissociation constants for carbonic acid of Lueker et al., (2000), bisulfate of Dickson, (1990), hydrofluoric acid of Perez and Fraga, (1987), and the boron-to-chlorinity ratio of (Lee et al., 2010). (Sulpis et al., 2020) found that the carbonic acid dissociation constants of (Lueker et al., 2000) may underestimate pCO_2 in cold regions (below ~8°C), and therefore overestimate pH and CO_3^{2-}. However, we choose to use (Lueker et al., 2000) because they are recommended (Dickson et al., 2007; Woosley, 2021), continue to be the standard (Jiang et al., 2021; Lauvset et al., 2021), and are commonly used at high latitudes (Duke et al., 2021; Raimondi et al., 2019; Woosley et al., 2017). Furthermore, the difference between DIC(pH^{est},pCO_2) and discrete samples interpolated to moored instrument depth ranged from 266 to -195 umol/kg using the k1 k2 of (Sulpis et al., 2020), compared to -38 to -7 umol/kg using (Lueker et al., 2000).

2.8 Influence of freshwater and temperature on inorganic carbon system

Salinity influence on inorganic carbon system

Inorganic carbon chemistry at the CEO site can be influenced by freshwater from sea ice melt and meteoric sources (precipitation and rivers). The DIC and TA signatures within these different freshwater sources can vary significantly. TA and DIC concentrations of 450 µmol kg^{-1} and 400 µmol kg^{-1}, respectively, have been measured in Arctic sea ice (Rysgaard et al., 2007). The CEO site is influenced by upstream riverine sources in the Gulf of Alaska and Bering and Chukchi seas, and also at times by the Mackenzie River outflow from the eastern Beaufort Sea and the large Russian Arctic rivers located to the west of the Chukchi Sea. Riverine input along the Gulf of Alaska tends to have lower TA (366 µmol kg^{-1}) and DIC (397 µmol kg^{-1}) concentrations (Stackpoole et al., 2016, 2017) than rivers draining into the Bering, Chukchi, and Beaufort Seas (TA = 1860 µmol kg^{-1}, DIC = 2010 µmol kg^{-1}, Holmes et al., 2021). In order to

https://doi.org/10.5194/egusphere-2023-1386
Preprint. Discussion started: 11 July 2023

disentangle the effects of freshwater from other physical-biogeochemical drivers on the inorganic carbon system, it is common practice to salinity-normalize inorganic carbon parameters and nutrient concentrations to a reference salinity (S_{ref} = mean salinity of the timeseries) using a non-zero freshwater endmember as described in (Friis, 2003):

nP = (P -P(s=0))/S* Sref +P(s=0),

where P is the parameter to be normalized to a reference salinity. However, because of the various freshwater sources with large differences in biogeochemical signatures, determination of the freshwater endmembers of the system is not straightforward or even possible. In an attempt to find the most appropriate representative bulk freshwater endmember for TA, DIC, pCO_2, and NO_3, we determined the intercept of a regression line across the full timeseries. Comparison of normalized (n) nDIC, nTA, npCO_2, and nNO_3 with the non-normalized variables suggests that the large pCO_2 and pH changes in spring, summer, and fall are not driven by freshwater (S3).

Temperature influence on inorganic carbon system

Temperature at 33 m depth at the CEO site varied between -1.7 °C during the sea ice covered months and 4 °C in late fall in some years. The impact of these large temperature swings was analyzed by temperature normalizing pCO_2 ($pCO_{2,NT}$) following Takahashi et al., (2002):

$pCO_{2,NT} = pCO_2 * \exp(0.0423(T_{ref} - T))$;

where T_{ref} is the average temperature across the full timeseries (S4). Steep temperature increases occur during late fall during wind events, when warm and pCO_2 deplete surface waters are entrained to the instrument depth at 33 m (see section 3.1 for a more in-depth discussion of these mixing events). Since the thermal effect on pCO_2 is minimal compared to the effect of the mixing event and does not play a major role throughout the rest of the timeseries it is not visualized in the following figures and analysis.

2.9 Sea ice concentration

Sea ice concentration at the observatory site was taken from the National Snow and Ice Data Center (NSIDC; DiGirolamo et al., 2022). Latitude and longitude coordinates were converted to NSIDC's EASE grid coordinate system (Brodzik and Knowles, 2002) and the 25-km gridded data were bilinearly interpolated to calculate sea ice concentration at each point. Low sea ice is defined by < 51% sea ice coverage per grid cell.

https://doi.org/10.5194/egusphere-2023-1386
Preprint. Discussion started: 11 July 2023

2.10 Estimation of model-based ocean acidification trend

Model results were obtained from historical simulations of five different global Earth System Models: 1) GFDL-CM4 (Silvers et al., 2018), 2) GFDL-ESM4 (Horowitz et al., 2018), 3) IPSL-CM6A-LR-INCA (Boucher et al., 2020), 4) CNRM-ESM2-1 (Seferian, 2019), and 5) Max Plank Earth System Model 1.2 (MPI-ESM1-2-LR, Mauritsen et al., 2019) that are part of the Coupled Model Intercomparison Project Phase 6 (CMIP6). Each simulation was used to calculate the annual trend of aragonite saturation state and pH at the closest depth and grid cell to the CEO mooring.

3. Results

The sub-surface waters at the CEO site comprise a high pCO_2, low pH, and low Ω_{arag} environment, with mean values of pCO_2^{mean} = 538 µatm , pH^{mean} = 7.91, Ω_{arag}^{mean} = 0.94 across the full data record (Figure 2 d,e,k). Spikes of high pH and Ω_{arag} and low pCO_2 occur in spring and fall; we define these spikes as relaxation events (see discussion for justification of term).

3.1 Divers of relaxation events

Spring: Springtime relaxation events at 33 m depth that exhibit relatively higher pH and Ω_{arag} and lower pCO_2 are likely consequences of the dissolution of $CaCO_3$ minerals and photosynthetic activity during sea ice break-up (Figure 2). In June of 2019 and 2020, near bottom pH and Ω_{arag} spiked to > 8.17 and > 1.5, respectively, while pCO_2 dropped to < 286 µatm. Ω_{arag} remained oversaturated and pH was greater than 8.0 for nearly all of June in 2018. In 2019, the relaxation event was less sustained, with only four short (2-6 day-long) events of relatively higher pH and Ω_{arag} > 1 in June and July. In both years, these events were characterized by a sudden increase in TA (Figure 2i) and decrease in DIC (Figure 2j) in a sea ice melt affected area and therefore presumably well stratified water column.

In 2018, O_2 increased by 74 umol kg^{-1} and chlorophyll fluorescence spiked (Figure 2g & h), both signs of photosynthetic activity. Assuming that 150 umol kg^{-1} of O_2 are produced per 106 umol kg^{-1} of DIC (Laws, 1991) consumed, DIC must have decreased by 53 umol kg^{-1} as a result of organic matter formation. However, we see a decrease of 39 umol kg^{-1} DIC over this period. With NO_3 assumed as the nitrogen source for the organic matter formation and a Redfield

https://doi.org/10.5194/egusphere-2023-1386
Preprint. Discussion started: 11 July 2023

stoichiometry of 6.6 mol C per mol N, TA should have increased by ~8 umol kg^{-1} (+ 0.15 umol TA per umol DIC consumed). However, the observed TA increase was 35 umol kg^{-1}, suggesting that $CaCO_3$ mineral dissolution led to an increase of 27 umol kg^{-1} in TA. Since dissolution of $CaCO_3$ increases TA twice as much as DIC (Sarmiento and Gruber, 2006), this process must have added ~13.5 umol kg^{-1} to DIC, which explains the lower-than-expected decrease in DIC (39 umol kg^{-1}).

A similar exercise can be undertaken for 2019, except using NO_3 since we don't have O_2 data available for that time. In the following we will again assume that NO_3 is the primary source of nitrogen during organic matter formation, and that assimilation of 1 umol of NO_3 leads to an increase of TA of 1 umol (Wolf-Gladrow et al., 2007). Based on the observed NO_3 decrease of 7.6 umol kg^{-1} and if DIC and TA were changed solely by organic matter formation we would expect an increase of TA by 7.6 umol kg^{-1} and DIC by ~50 umol kg^{-1}. As in 2018, the associated increase in TA of 23 umol kg^{-1} is larger than expected from organic matter formation alone and is likely due to $CaCO_3$ mineral dissolution. Roughly 15.4 umol kg^{-1} of TA change would then be due to dissolution of $CaCO_3$, which would contribute about 7.7 umol kg^{-1} to DIC, explaining the smaller-than-expected decrease in DIC. Since the water column is expected to be well-stratified during this time of the year it is unlikely that gas exchange has appreciable influence on DIC at 33 m depth.

Fall: The relaxation events in fall were characterized by large and sudden drops in CO_2, abrupt increases in pH and Ω_{arag}, and considerable interannual variability in their timing. Unlike relaxation events observed in spring, we're attributing these fall relaxation events to wind-induced physical mixing. To examine the controlling mechanisms causing these abrupt relaxation events in fall, we will start with using water column salinity and temperature data from a freeze-up detection buoy (Hauri et al., 2018) that was deployed in summer 2017 approximately 1 km away from the biogeochemical mooring. The freeze-up detection mooring provided temperature and salinity measurements every 7 meters throughout the water column from the time of its deployment in mid-August until freeze-up. Data from the freeze-up detection mooring suggest that warmer and fresher water from the upper water column gets periodically entrained down to the location of the biogeochemical sensor package at 33 m depth, leading to enhanced variability of density in August and September (Figure 6). During this time pCO_2 often decreased to or below atmospheric levels and pH sporadically reached values > 8. At the end of

https://doi.org/10.5194/egusphere-2023-1386
Preprint. Discussion started: 11 July 2023

September, a strong mixing event homogenized the water column from the surface down to the location of the sensor package and caused a sudden temperature to increase from 0.4 °C to 3.9 °C (Figure 6a and 7a). At the same time, pCO_2 decreased from 590 to 308 µatm. This suggests that warm and CO_2-deplete surface water replaced the CO_2-rich subsurface water and led to a sustained relaxation period that subsequently lasted until mid-November. Another mixing event further eroded the water column and replaced subsurface water with colder and fresher water (ice melt) from the surface at the end of October. This second large mixing event did not lead to large changes in pCO_2, pH, and Ω_{arag}.

Salinity and temperature records from the biogeochemical mooring at 33 m depth also suggest fall season mixing events in all other years, when increases in temperature coincide with decreases in pCO_2 (Figure 7). For example, two mixing events shaped the carbonate chemistry evolution in fall 2018. pCO_2 decreased from 915 µatm to around 565 µatm and Ω_{arag} increased to 0.9 as temperature increased and salinity decreased in early September (Figure 7). pCO_2 then increased to 1160 µatm in late October, before decreasing to 385 µatm at the beginning of November, causing a spike in Ω_{arag} to 1.34. At the same time, salinity decreased by 1 unit, suggesting a strong mixing event. Throughout November 2018, pCO_2 oscillated between 344 and 757 µatm and salinity between 31.01 and 32.97, hinting at additional mixing.

Similarly, an early mixing event in 2019 decreased pCO_2 to 352 µatm at the beginning of September. Short-term variability in pCO_2 with maximum levels of up to 855 µatm and minimum values below 300 µatm, variable temperature and salinity, and sporadic aragonite oversaturation events point to mixing through mid-September. At the end of October a large mixing event homogenized the water column that was accompanied by a decline of salinity by >1 unit, increase of temperature to 4 °C, and decrease of pCO_2 from 565 µatm to below 400 µatm . In a similar fashion to 2018, this fall mixing event was followed by a month-long period of large variability of pCO_2, salinity, pH, and Ω_{arag}, leading to short and sporadic aragonite oversaturation events in November, and a sustained oversaturation in December.

3.2 Drivers of sustained periods of low pH and Ω_{arag}, and high pCO_2

Summer through late fall: Bottom waters at the CEO site were most acidified during the sea ice free periods in summer through late fall. pH and Ω_{arag} started to gradually decrease at the beginning of July in 2018 and reached an annual low at the beginning of November (Ω_{arag_min} =

https://doi.org/10.5194/egusphere-2023-1386
Preprint. Discussion started: 11 July 2023

0.47, pH_{min} = 7.58, Figure 2 e & k). In November, the waters were also undersaturated with regards to calcite (not shown) and pCO_2 peaked at 1159 µatm (Figure 2d). The gradual decrease of pH and Ω_{arag} and increase of pCO_2 was interrupted by a strong mixing event in September, which entrained warmer, fresher, and CO_2-poor water down to 33 m depth (section 3.1). Dissolved oxygen decreased from 592 umol kg^{-1} at the beginning of July to 290 umol kg^{-1} before this first mixing event. At the same time DIC increased from 2074 umol kg^{-1} to 2197 umol kg^{-1} and TA increased by 4 umol kg^{-1}. Applying the oxygen to carbon ratio by Laws (1991) suggests a 215 umol kg^{-1} increase of DIC and a 33 umol kg^{-1} decrease of TA due to remineralization. However, TA increased by 4 umol kg^{-1}, suggesting $CaCO_3$ dissolution, which may have added ~37 umol kg^{-1} to TA and roughly 18.5 umol kg^{-1} to DIC. This scaling overestimates the observed DIC increase by 111 umol kg^{-1} and points to the likely influence of gas exchange. After the wind event, O_2 dropped from 408 umol kg^{-1} to 305 umol kg^{-1} when the O_2 sensor stopped working properly at the beginning of October. Applying the oxygen to carbon ratio by (Laws, 1991) again we would expect remineralization to increase DIC by 74 umol kg^{-1} and decrease TA by 11 umol kg^{-1}. However, observations suggest an increase in TA by 12 umol kg^{-1}, hinting again to $CaCO_3$ dissolution and thereby adding 23 umol kg^{-1} to TA and 11.5 umol kg^{-1} to DIC. The expected 85.5 umol kg^{-1} increase of DIC as a result of remineralization and $CaCO_3$ dissolution overestimates the observed DIC change by 9.5 umol kg^{-1}, again likely due to the uptake of CO_2 from the atmosphere.

The 2019 observations paint a similar picture of remineralization, $CaCO_3$ dissolution, and uptake of atmospheric CO_2 during the summer months. Between the end of June and end of August, NO_3 increased by 9.6 umol kg^{-1}. If DIC and TA were solely affected by remineralization of organic matter, we would expect an increase of DIC by 63.4 umol kg^{-1} and a decrease of TA by 9.6 umol kg^{-1}. The observed increase in TA can only be explained by $CaCO_3$ dissolution of ~24 umol kg^{-1}, which would add ~12 umol kg^{-1} to DIC. The combined effects of remineralization and dissolution would sum up to an expected increase in DIC of 76 umol kg^{-1}. This overestimates the observed DIC increase by 17 umol kg^{-1}, and may again be the result of atmospheric CO_2 uptake.

Winter: pCO_2 steadily increased and pH and Ω_{arag} decreased during the sea ice covered periods. pH was < 8 and aragonite remained undersaturated under the sea ice. At the same time, NO_3 slowly increased and O_2 decreased, which points to slow organic matter remineralization

https://doi.org/10.5194/egusphere-2023-1386
Preprint. Discussion started: 11 July 2023

(Figure 8). Short-term variability in salinity, especially in January 2019 and 2020 suggests the influence of different water masses, which was also reflected in TA, DIC, and NO_3 (Figures 8 and S3).

3.3 Summer of 2020 was different

Sea ice break-up did not lead to a spring relaxation event in 2020. On the contrary, pCO_2 gradually increased by roughly 200 µatm throughout the sea ice covered months to 650 µatm when sea ice started to retreat at the beginning of July. By the end of July, pCO_2 peaked at 1389 µatm. At the same time, TA increased by 32 umol kg^{-1} and DIC increased by 119 umol kg^{-1} and NO_3 slightly decreased from 16 umol kg to 14 umol kg^{-1}. The increase of TA and relatively high increase of DIC provide evidence for a combination of $CaCO_3$ dissolution and remineralization. Since NO_3 slightly decreased rather than increased, it is possible that NO_3 was consumed through water column denitrification or modified by advection of water, however we do not have sufficient evidence to support either hypothesis.

4. Discussion

CEO data provide new insights into the synoptic, seasonal and interannual variability and controls of the inorganic carbon system in a time when ocean acidification and climate change have already started to transform this area. The observations suggest that the CEO site is a high-CO_2 and low-pH and low-Ω_{arag} environment most of the time, except during sea ice break-up when the combined effects of photosynthetic activity and $CaCO_3$ dissolution remove CO_2 and add alkalinity to the system, and later in fall, when strong storm events entrain CO_2-deplete surface waters to the seafloor. Lowest pH and $CaCO_3$ saturation states and highest pCO_2 occur in summer through late fall when organic matter remineralization dominates the carbonate system balance. During this time, Ω_{arag} can fall below 0.5 and even Ω_{calc} becomes sporadically undersaturated ($\Omega_{calc} < 1$).

4.1 Progression of ocean acidification in the Chukchi Sea

The Arctic Ocean acidification rate will continue to exceed the rate of CO_2 change in the atmosphere as a result of the impacts of freshening and other more localized, seasonal or short-term consequences of climate change (Woosley and Millero, 2020; Terhaar et al., 2021; Orr et

https://doi.org/10.5194/egusphere-2023-1386
Preprint. Discussion started: 11 July 2023

al., 2022; Qi et al., 2017). As a result, uncertainty in the rate of change pH and Ω_{arag} in the Chukchi Sea remains (pH: -0.0031 ± 0.0024 vs. -0.0047 ± 0.0026; $\Omega_{arag:}$ -0.0009 ± 0.0138 vs -0.017 ± 0.009, Qi et al., 2022a, b). The weaker trend was calculated with data starting in 1994, whereas the stronger trend used data starting eight years later. The difference is likely due to the regions' large spatial and temporal variability, limited spatial data coverage, and short timeframe of historic data (and thus statistically insignificant *p*-values), but it also provides evidence that climate change has accelerated the rate of ocean acidification over time. As a comparison, an average across historic simulations from five CMIP6 models (see methods) projects a change in pH of -0.0077 year^{-1} and Ω_{arag} of -0.0063 year^{-1} at the CEO site between 2002 – 2014 and a weaker trend between 1994-2014 (pH: -0.0025 year^{-1}; Ω_{arag}: -0.0021 year^{-1}). The historic simulations end in 2014 and therefore miss the last years of extreme sea ice loss. Both observations and global model-based trend estimates must be used with caution. Longer-term observations are only available from the sea ice free period, and therefore do not depict an annually representative trend. Global models do not resolve important local physical, chemical, and biological meso-scale processes and therefore mask out the variability of the inorganic carbon system and effects of climate change.

Organisms living at the CEO site may have always been exposed to large seasonal variability and low pH and Ω_{arag} (high pCO_2), but the combined effects of climate change and ocean acidification have rapidly made these conditions more extreme and longer-lasting. Ocean acidification serves as a gradual environmental press by increasing the system's mean and extreme pCO_2 and decreasing mean and extreme pH and Ω_{arag}. Climate induced changes to other important controls of the inorganic carbon system, such as sea ice, riverine input, temperature, and circulation can act as sudden pulses and further modulate the inorganic carbon system to a less predictable degree and cause extreme events (Woosley and Millero, 2020; Orr et al., 2022; Hauri et al., 2021; Qi et al., 2017). Huntington et al., (2020) describe a sudden and dramatic shift of the physical, biogeochemical and ecosystem conditions in the Chukchi and Northern Bering seas in 2017. For example, satellite data for the CEO site illustrate that the longest open water seasons on record occurred between 2017 and 2020. Before 2017, the open water season was on average 96 (+/- 32) days long (i.e., below 51 % concentration), of which 35 (+/-36) days were ice free, whereas between 2017 and 2020, the low sea ice period was 151 (+/- 27) days long, of which 112 (+/- 31) days were ice free (Figure 9). Sea ice decline and increased nutrient influx

https://doi.org/10.5194/egusphere-2023-1386
Preprint. Discussion started: 11 July 2023

has also promoted increased phytoplankton primary production in the area (Lewis et al., 2020; Arrigo and van Dijken, 2015; Payne et al., 2021). Since our inorganic carbon time series started after the "dramatic shift" that was observed in the Chukchi Sea in 2017 (Huntington et al., 2020) and given the uncertainty in model output in this region, we can only speculate about how the changes in sea ice, temperature and biological production may have affected seasonal variability and extremes of the inorganic carbon chemistry at the CEO site. However, since the summertime low pH and Ω_{arag} and high pCO_2 are tightly coupled to the length of the ice-free period and intensity of organic matter production, it is possible that the observed summertime period of extreme conditions may have been previously unexperienced at this site. We therefore think it is justified to call the spikes of pH and Ω_{arag} "ocean acidification relaxation events", since the long-lasting summertime period of extremely low pH and Ω_{arag} maybe be a new pattern.

4.2 Relevance for ecosystem

Marine organisms are exposed to a wide range of naturally fluctuating environmental conditions such as temperature, salinity, carbonate chemistry and food concentrations that together constitute their ecological niche. As evolution works toward adaptation, the tolerance range of species and ecosystems to such parameters varies between locations and is often closely related to niche status. Stress can be defined as a condition evoked in an organism by one or more environmental and biological factors that bring the organism near or over the limits of its ecological niche (after Van Straalen, 2003). The consequence of the exposure to a stressor will depend on organismal sensitivity, stress intensity (how much it deviates from present conditions) and stress duration. In a synthesis of the global literature on the biological impacts of ocean acidification, Vargas et al. (2017, 2022) showed that the extreme of the present range of variability of carbonate chemistry is a good predictor of species sensitivity. In other words, larger deviations from present extreme high pCO_2 or extreme low pH, exert more negative biological impacts. Organismal stress and niche boundaries have implications for the definition and understanding of controls and future ocean acidification conditions in experiments aimed at evaluating future biological impacts.

Our data provide insights on conditions that affect and determine local species' ecological niches, and a necessary key is to evaluate or re-evaluate their sensitivity to present and future carbonate chemistry conditions. For example, an experimental study on 3 common Arctic

https://doi.org/10.5194/egusphere-2023-1386
Preprint. Discussion started: 11 July 2023

bivalve species (*Macoma calcarean, Astarte montagui* and *Astarte borealis*) collected in the CEO concluded that these species were generally resilient to decreasing pH (Goethel et al., 2017). However, only two pH were compared (a "control" (pH 8.1) and an "acidified" treatment (pH 7.8) and our results show that organisms are experiencing more extreme conditions already today. While these data are providing insights on these species' plasticity to present pH conditions, they cannot be used to infer sensitivity to future ocean acidification or extremes of today's conditions. Based on the local adaptation hypothesis (Vargas et al. 2017, 2022), stress and associated negative effect on species fitness can be expected when pH deviates from the extreme of the present range of variability (pH<7.5) as shown in other regions (e.g. echinoderms: Dorey et al., (2013); crustaceans: Thor and Dupont, (2015); bivalves: Ventura et al., 2016).

In the CEO, our results show sustained periods of remarkably low pH (e.g., 7.5; summer to fall, winter). Higher pH values are observed in spring and late fall. While we are lacking the local biological data to sufficiently evaluate past and future ecosystem changes, a high rate of ocean acidification as observed in the Chukchi Sea (Qi et al., 2022b, a), associated with potential temperature-induced shifts in the carbonate chemistry cycle (e.g. Orr et al. 2022), have the potential to drive negative impacts on species and ecosystems. Exposure to low pH increases organismal energy requirements for maintenance (e.g. acid-base regulation Stumpp et al., (2012), compensatory calcification (Ventura et al., 2016). Organisms can cope with increased energy costs using a variety of strategies, ranging from individual physiological to behavioral responses, depending on trophic level, mobility, and other ecological factors. For example, they can use available stored energy to compensate for increased costs or they can decrease their metabolism to limit costs (AMAP 2018). At the CEO, the low pH period observed during the summer and fall is associated with elevated temperature and an elevated food supply for herbivores (Lalande et al., 2020). The high availability of food may then foster compensation for the higher energetic costs associated with exposure to low pH. However, a longer period of low pH as suggested by our data could lead to a mismatch between the low pH and food availability, with cascading negative consequences for the ecosystem (Kroeker et al., 2021). In winter, the low pH conditions are associated with low temperature, no light, and low food level concentrations. These conditions are likely to keep metabolisms low and limit the negative effects of exposure to low pH (e.g. Gianguzza et al., (2014). As food availability is limited by the absence of light, this strategy may be compromised by an increase in temperature that could also lead to increased

https://doi.org/10.5194/egusphere-2023-1386
Preprint. Discussion started: 11 July 2023

metabolism. Additional work is needed to understand impacts of acidification conditions and variability on the marine biota of the Chukchi Sea, including field and laboratory experiments that evaluate biological response under realistic scenarios. The characterization of the environmental conditions at the CEO, including the variability in time, can be used to design single and multiple stressors experiments (carbonate chemistry, temperature, salinity, food, oxygen; Boyd et al. 2018).

Indigenous communities are at the forefront of the changing Arctic, including changes in accessibility, availability, and condition of traditional marine foods (Buschman and Sudlovenick, 2022; Hauser et al., 2021). We showed seasonal and interannual variation in carbonate conditions that have the potential to impact species critical to the food and cultural security of coastal Inupiat who have thrived in Arctic Alaska for millenia. For example, we have characterized seasonal low pH conditions that could impact organisms like bivalves in a foraging hotspot for walrus (Jay et al., 2012; Kuletz et al., 2015). Walrus, as well as their bivalve stomach contents, are important nutritional, spiritual, and cultural components, raising concerns for food security in the context of ecosystem shifts associated with the variability and multiplicity of climate impacts within the region (ICC, 2015).

4.3 Near-bottom photosynthetic activity, and $CaCO_3$ dissolution

The springtime relaxation events in 2018 and 2019 with relatively higher pH and Ω_{arag}, and lower pCO_2, was driven by a combination of photosynthetic activity and $CaCO_3$ dissolution. Near bottom photosynthetic activity has been observed at different locations across the Chukchi Sea and is likely due in part to sea ice algae that sink through the water column to the seafloor as sea ice retreats and continues to photosynthesize there for weeks (Stabeno et al., 2020; Koch et al., 2020). Sediment trap data from a CEO deployment prior to the start of this pCO2 and pH time-series suggest that export of the exclusively sympagic sea ice algae Nitzschia frigida peaked in May and June, during snow and ice melt events (Lalande et al., 2020).

The observed $CaCO_3$ mineral dissolution at the CEO site are likely driven by ikaite crystal dissolution in spring and aragonite and calcite dissolution in summer and fall. In spring, TA increased while both aragonite and calcite were supersaturated. Thus, the chemical dissolution of aragonite and calcite is not possible. The observed spike in TA happened in conjunction with sea ice break up. We therefore hypothesize that ikaite crystals that were trapped

https://doi.org/10.5194/egusphere-2023-1386
Preprint. Discussion started: 11 July 2023

in the ice matrix during brine rejection dissolved in the water column when sea ice melted, as was found in other areas of the Arctic (Rysgaard et al., 2012, 2007). On the other hand, aragonite and calcite undersaturation during sea ice free periods likely triggered $CaCO_3$ mineral dissolution and led to increases in TA. Shallow $CaCO_3$ mineral dissolution has also been found south of the CEO, in Anadyr waters in the Bering Sea and was also attributed to summertime organic matter remineralization (Cross et al., 2013).

4.4 Water column denitrification

Our inorganic carbon and nutrient timeseries provide indirect evidence of water column denitrification (section 3.3). The CEO salinity and temperature record suggest a resuspension event (increase in density) prior to the steep increase of pCO_2, DIC and TA and slight decrease of NO_3 in July of 2020. Zeng et al., (2017) have recorded high summertime denitrification activity in the oxic water column on the Chukchi Shelf and hypothesized that resuspension of benthic particles with bacteria may induce this active denitrification process. Water column denitrification would not only eliminate bio-available nitrogen from the Chukchi Sea, but it would also contribute to the outgassing of nitrous oxide and therefore climate change (Etminan et al., 2016).

4.5 pH algorithm

Deploying oceanographic equipment in remote Arctic locations is challenging. The data return from the SeapHOx sensors was minimal, despite annual servicing and calibration at Seabird. Our new pH algorithm is therefore all the more important as it fills important pH data gaps in the CEO timeseries. While we need another successful year of moored pH data return to fully evaluate our algorithm throughout the year, comparison with single discrete water samples nearby the CEO site and cruise datasets from the Chukchi Sea (Section 2.6, Table 2, Figures 5 and S1) suggest that our algorithm-derived pH falls within the weather quality goal of +/- 0.003 (Newton et al., 2015). The algorithm generally overestimates pH 0.0008 (Figures 3 and 4c), which means that the Ω_{arag} is also somewhat overestimated throughout the manuscript. Empirical relationships for estimating water column pH that rely on dissolved oxygen often ignore surface waters to limit biases due to decoupling the stoichiometry of the O_2:CO_2 relationship due to air-gas exchange (e.g. Juranek et al., 2011; Alin et al., 2012; Li et al., 2016). We see evidence of

https://doi.org/10.5194/egusphere-2023-1386
Preprint. Discussion started: 11 July 2023

this bias in our algorithm at low salinity (Figure 5c) and low pCO_2 (not shown) when compared with discrete samples collected across the arctic and from the surface to 500m (dataset described in Section 2.4), with pH^{disc}_{est} overestimating pH^{disc}_{calc} by a maximum of 0.053. If depth is restricted to between 30 and 500m when evaluating the algorithm with the same dataset described in Section 2.6, algorithm performance improves ($r^2 = 0.9990$, RMSE = 0.0055, p-value < 0.0001; not shown) and the maximum pH^{disc}_{est} overestimates by pH^{disc}_{calc} is 0.022. The combination of our new algorithm with recent progress in monitoring pCO_2 with Seagliders (Hayes et al., 2022) will further increase our ability to study the inorganic carbon dynamics at times and locations when shipboard or mooring based measurements may not be practical. Additional assessment is needed to determine to what degree the algorithm needs adjustments elsewhere.

Inherent spatial and temporal variability of the inorganic carbon parameters in the Chukchi Sea make the use of discrete water samples for evaluating sensor-based measurements difficult. Historic continuous surface measurements from the area suggest that surface pCO_2 can be as low < 250 µatm in early fall (Hauri et al., 2013), at a time of year when subsurface pCO_2 reaches its max of >800 µatm at the CEO site. This suggests a steep pCO_2 gradient of > 17 µatm per meter. High-resolution pH data from the 2017/2018 deployment suggests high temporal variability as well, further complicating the collection of discrete water samples to adequately evaluate the sensors. The HydroC's zeroing function, in addition to our pre and post calibration routines that factor into the post-processing of the data gives us confidence in the accuracy of the data.

5. Concluding Thoughts

The Chukchi Sea is undergoing a rapid environmental transformation with potentially far-reaching consequences across the ecosystem. While we are lacking a long-term time-series, we used this data set to understand the drivers of extreme pH, Ω_{arag}, and pCO_2 and document conditions that could affect the ecological niches of organisms, including a fast rate of ocean acidification, elongated sea ice free periods, increased primary productivity and elevated temperature. While a combination of experimental and monitoring approaches is needed for an understanding of the ecological consequences of these changes, our results also highlight to urgency to mitigate CO_2 emissions and simultaneously support Indigenous-led conservation

https://doi.org/10.5194/egusphere-2023-1386
Preprint. Discussion started: 11 July 2023

measures to safeguard an ecosystem in transition. Indigenous People in the Arctic have established strategies to monitor, adapt to, and conserve the ecosystems upon which they depend. Ethical and equitable engagement of Indigenous Knowledge and the communities at the forefront of climate impacts can help guide research and conservation action by centering local priorities and traditional practices, thereby supporting self-determination and sovereignty (Buschman and Sudlovenick, 2022).

Data availability

The data used in this manuscript are publicly available (Hauri and Irving, 2023a; Hauri and Irving, 2023b).

Author contributions

CH and BI managed and serviced the HydroC CO2 and SeapHOx sensors, analyzed and published the data, and wrote the manuscript. RP, DH, SD, and SLD contributed to the manuscript.

Competing interests

The authors have no competing interests.

Acknowledgments

The Chukchi Ecosystem Observatory is located on the traditional and contemporary hunting grounds of the Northern Alaskan Iñupiat. We also acknowledge that our Fairbanks-based offices are located on the Native lands of the lower Tanana Dena. The Indigenous peoples of this land never surrendered lands or resources to Russia or the United States. We acknowledge this not only because we are grateful to the Indigenous communities who have been in deep connection with the land and water for time immemorial, but also in recognition of the historical and ongoing legacy of colonialism. We are committed to improving our scientific approaches and working towards co-production for a better future for everyone.

We acknowledge the World Climate Research Programme, which, through its Working Group on Coupled Modelling, coordinated and promoted CMIP6. We thank the climate modeling groups for producing and making available their model output, the Earth System Grid

https://doi.org/10.5194/egusphere-2023-1386
Preprint. Discussion started: 11 July 2023

Federation (ESGF) for archiving the data and providing access, and the multiple funding agencies who support CMIP6 and ESGF.

Financial support

We would like to thank the National Pacific Research Board Long-term Monitoring (NPRB LTM) program (project no. 1426 and L-36), the Alaska Ocean Observing System (award no. NA11NOS0120020 and NA16NOS0120027), and the University of Alaska Fairbanks for their financial support. Claudine Hauri, Brita Irving, and Seth Danielson also acknowledge support from the National Science Foundation Office of Ocean Sciences and Polar Programs (OCE-1841948 and OPP-1603116). Projects that serviced the CEO and/or collected water column calibration data were funded by the National Science Foundation, Bureau of Ocean Energy Management, National Oceanic and Atmospheric Administration, National Oceanographic Partnership Program, and Shell Exploration and Production Company, Inc. Maintenance and calibration of the CEO sensors is only possible due to the kind support of numerous collaborators within the Arctic research community who helped with CEO deployment and recovery or collected sensor calibration samples. We would therefore like to thank Carin Ashjian, Jessica Cross, Miguel Goñi, Jackie Grebmeier, Burke Hales, Katrin Iken, Laurie Juranek, Calvin Mordy, and Robert Pickart.

References

Alin, S. R., Feely, R. A., Dickson, A. G., Hernández-Ayón, J. M., Juranek, L. W., Ohman, M. D., and Goericke, R.: Robust empirical relationships for estimating the carbonate system in the southern California Current System and application to CalCOFI hydrographic cruise data (2005–2011), 2012.

AMAP Assessment 2018: Arctic Ocean Acidification | AMAP: https://www.amap.no/documents/doc/AMAP-Assessment-2018-Arctic-Ocean-Acidification/1659, 2023.

Arrigo, K. R. and van Dijken, G. L.: Continued increases in Arctic Ocean primary production, Prog. Oceanogr., 136, 60–70, https://doi.org/10.1016/j.pocean.2015.05.002, 2015.

Bednaršek, N., Calosi, P., Feely, R. A., Ambrose, R., Byrne, M., Chan, K. Y. K., Dupont, S., Padilla-Gamiño, J. L., Spicer, J. I., Kessouri, F., Roethler, M., Sutula, M., and Weisberg, S. B.: Synthesis of thresholds of ocean acidification impacts on echinoderms, 2021.

https://doi.org/10.5194/egusphere-2023-1386
Preprint. Discussion started: 11 July 2023

765
766 Bittig, H. C., Steinhoff, T., Claustre, H., Fiedler, B., Williams, N. L., Sauzède, R., Körtzinger,
767 A., and Gattuso, J.-P.: An alternative to static climatologies: robust estimation of open ocean
768 CO2 variables and nutrient concentrations from T, S, and O2 data using Bayesian neural
769 networks, Front. Mar. Sci., 5, 328, https://doi.org/10.3389/fmars.2018.00328, 2018.
770
771 Bresnahan, P. J., Martz, T. R., Takeshita, Y., Johnson, K. S., and LaShomb, M.: Best practices
772 for autonomous measurement of seawater pH with the Honeywell Durafet, Methods Oceanogr.,
773 9, 44–60, https://doi.org/10.1016/j.mio.2014.08.003, 2014.
774
775 Brodzik, M. J. and K. W. Knowles: "Chapter 5: EASE-Grid: A Versatile Set of Equal-Area
776 Projections and Grids." in Michael F.Goodchild (Ed.) Discrete Global Grids: A Web Book.
777 Santa Barbara, California USA: National Center for Geographic Information & Analysis.
778 https://escholarship.org/uc/item/9492q6sm, 2002.
779
780 Buschman, V. Q. and Sudlovenick, E.: Indigenous-led conservation in the Arctic supports global
781 conservation practices, Arct. Sci., https://doi.org/10.1139/as-2022-0025, 2022.
782
783 Carter, B. R., Feely, R. A., Williams, N. L. , Dickson, A. G., Fong, M. B., and Takeshita, Y.:
784 Updated methods for global locally interpolated estimation of alkalinity, pH, and nitrate,
785 Methods Limnology and Oceanography, 16(2), 119-131, https://doi.org/10.1002/lom3.10232,
786 2018.
787
788 Corlett and Pickart, 2017
789
790 Cross, J. N., Mathis, J. T., Bates, N. R., and Byrne, R. H.: Conservative and non-conservative
791 variations of total alkalinity on the Southeastern Bering Sea Shelf, Mar. Chem., 154, 100–112,
792 https://doi.org/10.1016/j.marchem.2013.05.012, 2013.
793
794 Cross, J. N.; Monacci, N. M.; Bell, S. W.; Grebmeier, J. M.; Mordy, C.; Pickart, R. S.; Stabeno,
795 and P. J.: Dissolved inorganic carbon (DIC), total alkalinity (TA) and other variables collected
796 from discrete samples and profile observations from United States Coast Guard Cutter (USCGC)
797 Healy cruise HLY1702 (EXPOCODE 33HQ20170826) in the Bering and Chukchi Sea along
798 transect lines in the Distributed Biological Observatory (DBO) from 2017-08-26 to 2017-09-15
799 (NCEI Accession 0208337). NOAA National Centers for Environmental Information. Dataset.
800 https://doi.org/10.25921/pks4-4p43, 2020a.
801
802 Cross, J. N.; Monacci, N. M.; Bell, S. W.; Grebmeier, J. M.; Mordy, C.; Pickart, R. S.; Stabeno,
803 P. J.. Dissolved inorganic carbon (DIC), total alkalinity (TA) and other parameters collected
804 from discrete sample and profile observations during the USCGC Healy cruise HLY1801

https://doi.org/10.5194/egusphere-2023-1386
Preprint. Discussion started: 11 July 2023

(EXPOCODE 33HQ20180807) in the Bering Sea, Chukchi Sea and Beaufort Sea along transect lines in the Distributed Biological Observatory (DBO) from 2018-08-07 to 2018-08-24 (NCEI Accession 0221911). NOAA National Centers for Environmental Information. Dataset. https://doi.org/10.25921/xc4b-xh20, 2020b.

Cross, J. N.; Monacci, N. M.; Bell, S. W.; Grebmeier, J. M.; Mordy, C.; Pickart, Robert S.; Stabeno, P.J.. Dissolved inorganic carbon (DIC) and total alkalinity (TA) and other hydrographic and chemical data collected from discrete sample and profile observations during the United States Coast Guard Cutter (USCGC) Healy cruise HLY1901 (EXPOCODE 33HQ20190806) in the Bering and Chukchi Sea along transect lines in the Distributed Biological Observatory (DBO) from 2019-08-06 to 2019-08-22 (NCEI Accession 0243277). NOAA National Centers for Environmental Information. Dataset. https://doi.org/10.25921/b5s5-py61, 2021.

Cullison-Gray, S. E., DeGrandpre, M. D., Moore, T. S., Martz, T. R., Friederich, G. E., and Johnson, K. S.: Applications of in situ pH measurements for inorganic carbon calculations, Mar. Chem., 125, 82–90, https://doi.org/10.1016/j.marchem.2011.02.005, 2011.

Daniel, A., Laës-Huon, A., Barus, C., Beaton, A. D., Blandfort, D., Guigues, N., Knockaert, M., Munaron, D., Salter, I., Woodward, E. M. S., Greenwood, N., and Achterberg, E. P.: Toward a Harmonization for Using in situ Nutrient Sensors in the Marine Environment, Front. Mar. Sci., 6, 773, https://doi.org/10.3389/fmars.2019.00773, 2020.

Danielson, S. L., Ahkinga, O., Ashjian, C., Basyuk, E., Cooper, L. W., Eisner, L., Farley, E., Iken, K. B., Grebmeier, J. M., Juranek, L., Khen, G., Jayne, S. R., Kikuchi, T., Ladd, C., Lu, K., McCabe, R. M., Moore, G. W. K., Nishino, S., Ozenna, F., Pickart, R. S., Polyakov, I., Stabeno, P. J., Thoman, R., Williams, W. J., Wood, K., and Weingartner, T. J.: Manifestation and consequences of warming and altered heat fluxes over the Bering and Chukchi Sea continental shelves, Deep Sea Res. Part II Top. Stud. Oceanogr., 177, 104781, https://doi.org/10.1016/j.dsr2.2020.104781, 2020.

Danielson, S.: (2021): Water temperature, conductivity, and others taken by CTD and Niskin bottles from the research vessel Norseman II Data for Arctic Marine Biodiversity Observing Network, AMBON, Program in the Chukchi Sea from 2017-08-07 to 2017-08-22 (NCEI Accession 0229072). NOAA National Centers for Environmental Information. Dataset. https://doi.org/10.25921/afz7-0d98, 2021.

Dickson, A. G.: Thermodynamics of the dissociation of boric acid in synthetic seawater from 273.15 to 318.15 K, Deep Sea Res. Part Oceanogr. Res. Pap., 37, 755–766, https://doi.org/10.1016/0198-0149(90)90004-F, 1990.

https://doi.org/10.5194/egusphere-2023-1386
Preprint. Discussion started: 11 July 2023

Dickson, A. G., Sabine, C. L., and Christian, J. R.: Guide to best practices for ocean CO2 measurements, PICES, Sydney, 191 pp., 2007.

DiGirolamo, N. E., C. L. Parkinson, D. J. Cavalieri, P. Gloersen, and H. J. Zwally. Sea Ice Concentrations from Nimbus-7 SMMR and DMSP SSM/I-SSMIS Passive Microwave Data, Version 2. [Indicate subset used]. Boulder, Colorado USA. NASA National Snow and Ice Data Center Distributed Active Archive Center. https://doi.org/10.5067/MPYG15WAA4WX, 2022.

Dorey, N., Lançon, P., Thorndyke, M., and Dupont, S.: Assessing physiological tipping point of sea urchin larvae exposed to a broad range of pH, Glob. Change Biol., 19, 3355–3367, https://doi.org/10.1111/gcb.12276, 2013.

Duke, P. J., Else, B. G. T., Jones, S. F., Marriot, S., Ahmed, M. M. M., Nandan, V., Butterworth, B., Gonski, S. F., Dewey, R., Sastri, A., Miller, L. A., Simpson, K. G., and Thomas, H.: Seasonal marine carbon system processes in an Arctic coastal landfast sea ice environment observed with an innovative underwater sensor platform, 2021.

Etminan, M., Myhre, G., Highwood, E. J., and Shine, K. P.: Radiative forcing of carbon dioxide, methane, and nitrous oxide: A significant revision of the methane radiative forcing, Geophys. Res. Lett., 43, 12,614-12,623, https://doi.org/10.1002/2016GL071930, 2016.

Fietzek, P., Fiedler, B., Steinhoff, T., and Körtzinger, A.: In situ quality assessment of a novel underwater CO2 sensor based on membrane equilibration and NDIR spectrometry, J. Atmospheric Ocean. Technol., 31, 181–196, https://doi.org/10.1175/JTECH-D-13-00083.1, 2014.

Friis, K.: The salinity normalization of marine inorganic carbon chemistry data, Geophys. Res. Lett., 30, 1085, https://doi.org/10.1029/2002GL015898, 2003.

Gianguzza, P., Visconti, G., Gianguzza, F., Vizzini, S., Sarà, G., and Dupont, S.: Temperature modulates the response of the thermophilous sea urchin Arbacia lixula early life stages to CO2-driven acidification, Mar. Environ. Res., 93, 70–77, https://doi.org/10.1016/j.marenvres.2013.07.008, 2014.

Goethel, C. L., Grebmeier, J. M., Cooper, L. W., and Miller, T. J.: Implications of ocean acidification in the Pacific Arctic: Experimental responses of three Arctic bivalves to decreased pH and food availability, Deep Sea Res. Part II Top. Stud. Oceanogr., 144, 112–124, https://doi.org/10.1016/j.dsr2.2017.08.013, 2017.

https://doi.org/10.5194/egusphere-2023-1386
Preprint. Discussion started: 11 July 2023

Gonzalez, S., Horne, J. K., and Danielson, S. L.: Multi-scale temporal variability in biological-physical associations in the NE Chukchi Sea, Polar Biol., 44, 837–855, https://doi.org/10.1007/s00300-021-02844-1, 2021.

Hauri, C., Danielson, S., McDonnell, A. M. P., Hopcroft, R. R., Winsor, P., Shipton, P., Lalande, C., Stafford, K. M., Horne, J. K., Cooper, L. W., Grebmeier, J. M., Mahoney, A., Maisch, K., McCammon, M., Statscewich, H., Sybrandy, A., and Weingartner, T.: From sea ice to seals: a moored marine ecosystem observatory in the Arctic, Ocean Sci., 14, 1423–1433, https://doi.org/10.5194/os-14-1423-2018, 2018.

Hauri, C., Pagès, R., McDonnell, A. M. P., Stuecker, M. F., Danielson, S. L., Hedstrom, K., Irving, B., Schultz, C., and Doney, S. C.: Modulation of ocean acidification by decadal climate variability in the Gulf of Alaska, 2021.

Hauri, C. and Irving, B.: pCO2 time series measurements from the Chukchi Ecosystem Observatory CEO2 mooring deployed at 33 meters depth in the Northeast Chukchi Sea. Research Workspace. https://doi.org/10.24431/rw1k7dq, version: 10.24431_rw1k7dq_20230531T123002Z, 2023.

Hauri, C. and Irving, B.: pH, temperature, salintiy, and oxygen time series measurements from the Chukchi Ecosystem Observatory CEO2 mooring deployed at 33 meters depth in the Northeast Chukchi Sea. Research Workspace. https://doi.org/10.24431/rw1k7dp , version: 10.24431_rw1k7dp_20230531T121136Z, 2023.

Hauser, D. D. W., Whiting, A. V., Mahoney, A. R., Goodwin, J., Harris, C., Schaeffer, R. J., Schaeffer, R., Laxague, N. J. M., Subramaniam, A., Witte, C. R., Betcher, S., Lindsay, J. M., and Zappa, C. J.: Co-production of knowledge reveals loss of Indigenous hunting opportunities in the face of accelerating Arctic climate change, Environ. Res. Lett., 16, 095003, https://doi.org/10.1088/1748-9326/ac1a36, 2021.

Hayes, D., Kemme, J., and Hauri C.: Ocean greenhouse gas monitoring: new autonomous platform to measure pCO_2, methane, Sea Technology, 63(10), 13-16, https://lsc-pagepro.mydigitalpublication.com/publication/?i=764237&p=13&view=issueViewer, 2022.

Hennon, T. D., Danielson, S. L., Woodgate, R. A., Irving, B., Stockwell, D. A., and Mordy, C. W.: Mooring Measurements of Anadyr Current Nitrate, Phosphate, and Silicate Enable Updated Bering Strait Nutrient Flux Estimates, Geophys. Res. Lett., 49, e2022GL098908, https://doi.org/10.1029/2022GL098908, 2022.

Holmes, R.M., J.W. McClelland, S.E. Tank, R.G.M. Spencer, and A.I. Shiklomanov. Arctic Great Rivers Observatory. Water Quality Dataset, https://www.arcticgreatrivers.org/data, 2021.

https://doi.org/10.5194/egusphere-2023-1386
Preprint. Discussion started: 11 July 2023

Huntington, H. P., Danielson, S. L., Wiese, F. K., Baker, M., Boveng, P., Citta, J. J., De Robertis, A., Dickson, D. M. S., Farley, E., George, J. C., Iken, K., Kimmel, D. G., Kuletz, K., Ladd, C., Levine, R., Quakenbush, L., Stabeno, P., Stafford, K. M., Stockwell, D., and Wilson, C.: Evidence suggests potential transformation of the Pacific Arctic ecosystem is underway, Nat. Clim. Change, 10, 342–348, https://doi.org/10.1038/s41558-020-0695-2, 2020.

ICC: Alaskan Inuit food security conceptual framework: how to assess the Arctic from an Inuit perspective, Inuit Circumpolar Council-Alaska, Anchorage, 2015.

Irving, B., SUNA_V2_processing, GitHub repository, https://github.com/britairving/SUNA_V2, 2021.

Jay, C. V., Fischbach, A. S., and Kochnev, A. A.: Walrus areas of use in the Chukchi Sea during sparse sea ice cover, Mar. Ecol. Prog. Ser., 468, 1–13, https://doi.org/10.3354/meps10057, 2012.

Jiang, L.-Q., Feely, R. A., Wanninkhof, R., Greeley, D., Barbero, L., Alin, S., Carter, B. R., Pierrot, D., Featherstone, C., Hooper, J., Melrose, C., Monacci, N., Sharp, J. D., Shellito, S., Xu, Y.-Y., Kozyr, A., Byrne, R. H., Cai, W.-J., Cross, J., Johnson, G. C., Hales, B., Langdon, C., Mathis, J., Salisbury, J., and Townsend, D. W.: Coastal Ocean Data Analysis Product in North America (CODAP-NA) – an internally consistent data product for discrete inorganic carbon, oxygen, and nutrients on the North American ocean margins, Earth Syst. Sci. Data, 13, 2777–2799, https://doi.org/10.5194/essd-13-2777-2021, 2021.

Juranek, L. W., Feely, R. A., Peterson, W. T., Alin, S. R., Hales, B., Lee, K., Sabine, C. L., and Peterson, J.: A novel method for determination of aragonite saturation state on the continental shelf of central Oregon using multi-parameter relationships with hydrographic data, Geophys. Res. Lett., 36, L24601, https://doi.org/10.1029/2009GL040778, 2009.

Juranek, L. W., Feely, R. A., Gilbert, D., Freeland, H., and Miller, L. A.: Real-time estimation of pH and aragonite saturation state from Argo profiling floats: Prospects for an autonomous carbon observing strategy, Geophys. Res. Lett., 38, L17603, https://doi.org/10.1029/2011gl048580, 2011.

Kroeker, K. J., Powell, C., and Donham, E. M.: Windows of vulnerability: Seasonal mismatches in exposure and resource identity determine ocean acidification's effect on a primary consumer at high latitude, Glob. Change Biol., 27, 1042–1051, https://doi.org/10.1111/gcb.15449, 2021.

Kuletz, K. J., Ferguson, M. C., Hurley, B., Gall, A. E., Labunski, E. A., and Morgan, T. C.: Seasonal spatial patterns in seabird and marine mammal distribution in the eastern Chukchi and

https://doi.org/10.5194/egusphere-2023-1386
Preprint. Discussion started: 11 July 2023

western Beaufort seas: Identifying biologically important pelagic areas, Prog. Oceanogr., 136, 175–200, https://doi.org/10.1016/j.pocean.2015.05.012, 2015.

Lalande, C., Grebmeier, J. M., Hopcroft, R. R., and Danielson, S. L.: Annual cycle of export fluxes of biogenic matter near Hanna Shoal in the northeast Chukchi Sea, Deep Sea Res. Part II Top. Stud. Oceanogr., 177, 104730, https://doi.org/10.1016/j.dsr2.2020.104730, 2020.

Lalande, C., Grebmeier, J. M., McDonnell, A. M. P., Hopcroft, R. R., O'Daly, S., and Danielson, S. L.: Impact of a warm anomaly in the Pacific Arctic region derived from time-series export fluxes, PLOS ONE, 16, e0255837, https://doi.org/10.1371/journal.pone.0255837, 2021.

Lauvset, S. K., Lange, N., Tanhua, T., Bittig, H. C., Olsen, A., Kozyr, A., Álvarez, M., Becker, S., Brown, P. J., Carter, B. R., Cotrim da Cunha, L., Feely, R. A., van Heuven, S., Hoppema, M., Ishii, M., Jeansson, E., Jutterström, S., Jones, S. D., Karlsen, M. K., Lo Monaco, C., Michaelis, P., Murata, A., Pérez, F. F., Pfeil, B., Schirnick, C., Steinfeldt, R., Suzuki, T., Tilbrook, B., Velo, A., Wanninkhof, R., Woosley, R. J., and Key, R. M.: An updated version of the global interior ocean biogeochemical data product, GLODAPv2.2021, Earth Syst. Sci. Data Discuss., https://doi.org/10.5194/essd-2021-234, 2021.

Laws, E. A.: Photosynthetic quotients, new production and net community production in the open ocean, Deep Sea Res. Part Oceanogr. Res. Pap., 38, 143–167, https://doi.org/10.1016/0198-0149(91)90059-O, 1991.

Lee, K., Kim, T.-W., Byrne, R. H., Millero, F. J., Feely, R. A., and Liu, Y.-M.: The universal ratio of boron to chlorinity for the North Pacific and North Atlantic oceans, Geochim. Cosmochim. Acta, 74, 1801–1811, https://doi.org/10.1016/j.gca.2009.12.027, 2010.

Lewis, E. and Wallace, D. W. R.: Program Developed for CO2 System Calculations, ORNL/CDIAC-105, Carbon Dioxide Inf. Anal. Cent., Oak Ridge Natl. Lab., Oak Ridge, Tenn., 38 pp., https://salish-sea.pnnl.gov/media/ORNL-CDIAC-105.pdf, 1998.

Lewis, K. M., van Dijken, G. L., and Arrigo, K. R.: Changes in phytoplankton concentration now drive increased Arctic Ocean primary production, Science, 369, 198–202, https://doi.org/10.1126/science.aay8380, 2020.

Li, B., Watanabe, Y. W., and Yamaguchi, A.: Spatiotemporal distribution of seawater pH in the North Pacific subpolar region by using the parameterization technique, J. Geophys. Res. Oceans, 121, 3435–3449, https://doi.org/10.1002/2015JC011615, 2016.

https://doi.org/10.5194/egusphere-2023-1386
Preprint. Discussion started: 11 July 2023

Licker, R., Ekwurzel, B., Doney, S. C., Cooley, S. R., Lima, I. D., Heede, R., and Frumhoff, P. C.: Attributing ocean acidification to major carbon producers, Environ. Res. Lett., 14, 124060, https://doi.org/10.1088/1748-9326/ab5abc, 2019.

Lueker, T. J., Dickson, A. G., and Keeling, C. D.: Ocean pCO2 calculated from dissolved inorganic carbon , alkalinity , and equations for K 1 and K 2 : validation based on laboratory measurements of CO2 in gas and seawater at equilibrium, Mar. Chem., 70, 105–119, https://doi.org/10.1016/S0304-4203(00)00022-0, 2000.

Martz, T. R., Connery, J. G., and Johnson, K. S.: Testing the Honeywell Durafet for seawater pH applications, Limnol. Oceanogr. Methods, 8, 172–184, https://doi.org/10.4319/lom.2010.8.172, 2010.

Mauritsen, T., Bader, J., Becker, T., Behrens, J., Bittner, M., Brokopf, R., Brovkin, V., Claussen, M., Crueger, T., Esch, M., Fast, I., Fiedler, S., Fläschner, D., Gayler, V., Giorgetta, M., Goll, D. S., Haak, H., Hagemann, S., Hedemann, C., Hohenegger, C., Ilyina, T., Jahns, T., Jimenéz-de-la-Cuesta, D., Jungclaus, J., Kleinen, T., Kloster, S., Kracher, D., Kinne, S., Kleberg, D., Lasslop, G., Kornblueh, L., Marotzke, J., Matei, D., Meraner, K., Mikolajewicz, U., Modali, K., Möbis, B., Müller, W. A., Nabel, J. E. M. S., Nam, C. C. W., Notz, D., Nyawira, S.-S., Paulsen, H., Peters, K., Pincus, R., Pohlmann, H., Pongratz, J., Popp, M., Raddatz, T. J., Rast, S., Redler, R., Reick, C. H., Rohrschneider, T., Schemann, V., Schmidt, H., Schnur, R., Schulzweida, U., Six, K. D., Stein, L., Stemmler, I., Stevens, B., von Storch, J.-S., Tian, F., Voigt, A., Vrese, P., Wieners, K.-H., Wilkenskjeld, S., Winkler, A., and Roeckner, E.: Developments in the MPI-M Earth System Model version 1.2 (MPI-ESM1.2) and Its Response to Increasing CO2, J. Adv. Model. Earth Syst., 11, 998–1038, https://doi.org/10.1029/2018MS001400, 2019.

McDougall, T.J. and P.M. Barker: Getting started with TEOS-10 and the Gibbs Seawater (GSW) Oceanographic Toolbox, 28pp., SCOR/IAPSO WG127, ISBN 978-0-646-55621-5, 2011.

McRaven, L. and R. Pickart: Conductivity-Temperature-Depth (CTD) data from the 2018 Distributed Biological Observatory - Northern Chukchi Integrated Study (DBO-NCIS) cruise on USCGC (US Coast Guard Cutter) Healy (HLY1801). Arctic Data Center. doi:10.18739/A2HT2GC7Z, 2021.

Monacci, N. M., Cross, J. N., Pickart, R. S., Juranek, L. W., McRaven, L. T., and Becker, S.: Dissolved inorganic carbon (DIC) and total alkalinity (TA) and other hydrographic and chemical data collected from discrete sample and profile observations aboard the RV Sikuliaq Cruise SKQ202014S (EXPOCODE 33BI20201025) in the Bering and Chukchi Sea along transect lines in the Distributed Biological Observatory (DBO) from 2020-10-25 to 2020-11-11 (NCEI

https://doi.org/10.5194/egusphere-2023-1386
Preprint. Discussion started: 11 July 2023

Accession 0252613). NOAA National Centers for Environmental Information. Dataset. https://doi.org/10.25921/pnsd-sv10, 2022.

Mordy, C. W., Bell, S., Cokelet, E. D., Ladd, C., Lebon, G., Proctor, P., Stabeno, P., Strausz, D., Wisegarver, E., and Wood, K.: Seasonal and interannual variability of nitrate in the eastern Chukchi Sea: Transport and winter replenishment, Deep-Sea Res. Part II Top. Stud. Oceanogr., 177, 104807, https://doi.org/10.1016/j.dsr2.2020.104807, 2020.

National Academies of Sciences, Engineering and Medicine: Valuing Climate Damages: Updating Estimation of the Social Cost of Carbon Dioxide (Washington DC: The National Academies Press) https://doi.org/10.17226/24651, 2017.

Newton, J. A., Feely, R. A., Jewett, E. B., Williamson, P., and Mathis, J.: Global ocean acidification observing network: requirements and governance plan, GOA-ON, Washington, 61 pp., 2015.

Orr, J. C.: Recent and future changes in ocean carbonate chemistry, in: Ocean acidification, edited by: Gattuso, J.-P. and Hansson, L., Oxford University Press, Oxford, 41–66, 2011.

Orr, J. C., Epitalon, J.-M., Dickson, A. G., and Gattuso, J.-P.: Routine uncertainty propagation for the marine carbon dioxide system, Mar. Chem., 207, 84–107, https://doi.org/10.1016/j.marchem.2018.10.006, 2018.

Orr, J. C., Kwiatkowski, L., and Pörtner, H. O.: Arctic Ocean annual high in pCO2 could shift from winter to summer, Nature, 610, 94–100, https://doi.org/10.1038/s41586-022-05205-y, 2022.

Payne, C. M., Bianucci, L., van Dijken, G. L., and Arrigo, K. R.: Changes in Under-Ice Primary Production in the Chukchi Sea From 1988 to 2018, J. Geophys. Res. Oceans, 126, e2021JC017483, https://doi.org/10.1029/2021JC017483, 2021.

Perez, F. F. and Fraga, F.: Association constant of fluoride and hydrogen ions in seawater, Mar. Chem., 21, 161–168, https://doi.org/10.1016/0304-4203(87)90036-3, 1987.

Qi, D., Chen, L., Chen, B., Gao, Z., Zhong, W., Feely, R. A., Anderson, L. G., Sun, H., Chen, J., Chen, M., Zhan, L., Zhang, Y., and Cai, W.-J.: Increase in acidifying water in the western Arctic Ocean, Nat. Clim. Change, 7, 195–199, https://doi.org/10.1038/nclimate3228, 2017.

Qi, D., Ouyang, Z., Chen, L., Wu, Y., Lei, R., Chen, B., Feely, R. A., Anderson, L. G., Zhong, W., Lin, H., Polukhin, A., Zhang, Y., Zhang, Y., Bi, H., Lin, X., Luo, Y., Zhuang, Y., He, J.,

https://doi.org/10.5194/egusphere-2023-1386
Preprint. Discussion started: 11 July 2023

Chen, J., and Cai, W. J.: Climate change drives rapid decadal acidification in the Arctic Ocean from 1994 to 2020, Science, 377, 1544–1550, https://doi.org/10.1126/science.abo0383, 2022a.

Qi, D., Wu, Y., Chen, L., Cai, W.-J., Ouyang, Z., Zhang, Y., Anderson, L. G., Feely, R. A., Zhuang, Y., Lin, H., Lei, R., and Bi, H.: Rapid acidification of the Arctic Chukchi Sea waters driven by anthropogenic forcing and biological carbon recycling, 2022b.

Raimondi, L., Matthews, J. B. R., Atamanchuck, D., Azetsu-Scott, K., and Wallace, D.: The internal consistency of the marine carbon dioxide system for high latitude shipboard and in situ monitoring, Mar. Chem., 213, 49–70, https://doi.org/10.1016/j.marchem.2019.03.001, 2019.

Rantanen, M., Karpechko, A. Y., Lipponen, A., Nordling, K., Hyvärinen, O., Ruosteenoja, K., Vihma, T., and Laaksonen, A.: The Arctic has warmed nearly four times faster than the globe since 1979, Commun. Earth Environ., 3, 1–10, https://doi.org/10.1038/s43247-022-00498-3, 2022.

Rysgaard, S., Glud, R. N., Sejr, M. K., Bendtsen, J., and Christensen, P. B.: Inorganic carbon transport during sea ice growth and decay: A carbon pump in polar seas, J. Geophys. Res., 112, C03016, https://doi.org/10.1029/2006JC003572, 2007.

Rysgaard, S., Glud, R. N., Lennert, K., Cooper, M., Halden, N., Leakey, R. J. G., Hawthorne, F. C., and Barber, D.: Ikaite crystals in melting sea ice – implications for pCO_2 and pH levels in Arctic surface waters, The Cryosphere, 6, 901–908, https://doi.org/10.5194/tc-6-901-2012, 2012.

Sakamoto, C. M., Johnson, K. S., and Coletti, L. J.: Improved algorithm for the computation of nitrate concentrations in seawater using an in situ ultraviolet spectrophotometer, Limnol. Oceanogr. Methods, 7, 132–143, https://doi.org/10.4319/lom.2009.7.132, 2009.

Sandy, S. J., Danielson, S. L., and Mahoney, A. R.: Automating the Acoustic Detection and Characterization of Sea Ice and Surface Waves, J. Mar. Sci. Eng., 10, 1577, https://doi.org/10.3390/jmse10111577, 2022.

Sarmiento, J. L. and Gruber, N.: Ocean Biogeochemical Dynamics, Princeton University Press, Princeton, NJ, 526 pp pp., 2006.

Seabird. Application Note 31: Computing temperature and conductivity slope and offset correction coefficients from lab calibration and salinity bottle samples. my.hach.com/asset-get.download.jsa?id=54627861537, accessed 20 June 2016.

https://doi.org/10.5194/egusphere-2023-1386
Preprint. Discussion started: 11 July 2023

Sea-Bird. Module 28. Advanced Biogeochemical Processing, www.seabird.com/cms-portals/seabird_com/cms/documents/training/Module28_Advanced_Biogeochem_Processing.pdf . Accessed 30 May 2023.

Semiletov, I., Pipko, I., Gustafsson, Ö., Anderson, L. G., Sergienko, V., Pugach, S., Dudarev, O., Charkin, A., Gukov, A., Bröder, L., Andersson, A., Spivak, E., and Shakhova, N.: Acidification of East Siberian Arctic Shelf waters through addition of freshwater and terrestrial carbon, Nat. Geosci., 9, 361–365, https://doi.org/10.1038/ngeo2695, 2016.

Serreze, M. C. and Barry, R. G.: Processes and impacts of Arctic amplification: A research synthesis, Glob. Planet. Change, 77, 85–96, https://doi.org/10.1016/j.gloplacha.2011.03.004, 2011.

Serreze, M. C. and Francis, J. A.: The arctic amplification debate, Clim. Change, 76, 241–264, https://doi.org/10.1007/s10584-005-9017-y, 2006.

Serreze, M. C., Crawford, A. D., Stroeve, J. C., Barrett, A. P., and Woodgate, R. A.: Variability, trends, and predictability of seasonal sea ice retreat and advance in the Chukchi Sea, J. Geophys. Res. Oceans, 121, 7308–7325, https://doi.org/10.1002/2016JC011977, 2016.

Sharp, J. D., Pierrot, D., Humphreys, M. P., Epitalon, J.-M., Orr, J. C., Lewis, E. R., and Wallace, D. W. R.: CO2SYSv3 for MATLAB, , https://doi.org/10.5281/zenodo.7552554, 2023.

Shu, Q., Wang, Q., Årthun, M., Wang, S., and Song, Z.: Arctic Ocean Amplification in a warming climate in CMIP6 models, 1–11, 2022.

Stackpoole, S., Butman, D., Clow, D., Verdin, K., Gaglioti, B., and Striegl, R. G.: Carbon burial, transport, and emission from inland aquatic ecosystems in Alaska, USGS Prof. Pap., 1826, 159–188, https://doi.org/10.3133/pp1826, 2016.

Stackpoole, S. M., Butman, D., Clow, D. W., Verdin, K. L., Gaglioti, B. V., Genet, H., and Striegl, R. G.: Inland waters and their role in the carbon cycle of Alaska, Ecol. Appl., 27, 1403–1420, http://onlinelibrary.wiley.com/doi/10.1002/eap.1552/full, 2017.

Stroeve, J. C., Serreze, M. C., Holland, M. M., Kay, J. E., Malanik, J., and Barrett, A. P.: The Arctic's rapidly shrinking sea ice cover: a research synthesis, Clim. Change, 110, 1005–1027, https://doi.org/10.1007/s10584-011-0101-1, 2011.

https://doi.org/10.5194/egusphere-2023-1386
Preprint. Discussion started: 11 July 2023

Stroeve, J. C., Markus, T., Boisvert, L., Miller, J., and Barrett, A.: Changes in Arctic melt season and implications for sea ice loss, Geophys. Res. Lett., 41, 1216–1225, https://doi.org/10.1002/2013GL058951, 2014.

Stumpp, M., Hu, M. Y., Melzner, F., Gutowska, M. A., Dorey, N., Himmerkus, N., Holtmann, W. C., Dupont, S. T., Thorndyke, M. C., and Bleich, M.: Acidified seawater impacts sea urchin larvae pH regulatory systems relevant for calcification, Proc. Natl. Acad. Sci. USA, 109, 18192–18197, https://doi.org/10.1073/pnas.1209174109, 2012.

Sulpis, O., Lauvset, S. K., and Hagens, M.: Current estimates of K1* and K2* appear inconsistent with measured CO2 system parameters in cold oceanic regions, Ocean Sci., 16, 847–862, https://doi.org/10.5194/os-16-847-2020, 2020.

Takahashi, T., Sutherland, S. C., Sweeney, C., Poisson, A., Metzl, N., Tilbrook, B., Bates, N., Wanninkhof, R., Feely, R. A., Sabine, C., Olafsson, J., and Nojiri, Y.: Global sea–air CO2 flux based on climatological surface ocean pCO2, and seasonal biological and temperature effects, Deep Sea Res. Part II Top. Stud. Oceanogr., 49, 1601–1622, https://doi.org/10.1016/S0967-0645(02)00003-6, 2002.

Terhaar, J., Torres, O., Bourgeois, T., and Kwiatkowski, L.: Arctic Ocean acidification over the 21st century co-driven by anthropogenic carbon increases and freshening in the CMIP6 model ensemble, Biogeosciences, 18, 2221–2240, https://doi.org/10.5194/bg-18-2221-2021, 2021.

Thomsen, J., Casties, I., Pansch, C., Körtzinger, A., and Melzner, F.: Food availability outweighs ocean acidification effects in juvenile Mytilus edulis: laboratory and field experiments, Glob. Change Biol., 19, 1017–1027, https://doi.org/10.1111/gcb.12109, 2013.

Thor, P. and Dupont, S.: Transgenerational effects alleviate severe fecundity loss during ocean acidification in a ubiquitous planktonic copepod, Glob. Change Biol., 21, 2261–2271, https://doi.org/10.1111/gcb.12815, 2015.

Tunnicliffe, V., Davies, K. T. A., Butterfield, D. A., Embley, R. W., Rose, J. W., and Chadwick Jr, W. W.: Survival of mussels in extremely acidic waters on a submarine volcano, Nat. Geosci., 2, 344–348, https://doi.org/10.1038/ngeo500, 2009.

Van Straalen, M. N.: Peer Reviewed: Ecotoxicology Becomes Stress Ecology, Environ. Sci. Technol., 37, 324A-330A, https://doi.org/10.1021/es0325720, 2003.

https://doi.org/10.5194/egusphere-2023-1386
Preprint. Discussion started: 11 July 2023

Vargas, C. A., Lagos, N. A., Lardies, M. A., Duarte, C., Manríquez, P. H., Aguilera, V. M., Broitman, B., Widdicombe, S., and Dupont, S.: Species-specific responses to ocean acidification should account for local adaptation and adaptive plasticity, 2017.

Vargas, C. A., Cuevas, L. A., Broitman, B. R., San Martin, V. A., Lagos, N. A., Gaitán-Espitia, J. D., and Dupont, S.: Upper environmental pCO2 drives sensitivity to ocean acidification in marine invertebrates, Nat. Clim. Change, 12, 200–207, https://doi.org/10.1038/s41558-021-01269-2, 2022.

Ventura, A., Schulz, S., and Dupont, S.: Maintained larval growth in mussel larvae exposed to acidified under-saturated seawater, Sci. Rep., 6, 23728, https://doi.org/10.1038/srep23728, 2016.

Watanabe, Y. W., Li, B. F., Yamasaki, R., Yunoki, S., Imai, K., Hosoda, S., and Nakano, Y.: Spatiotemporal changes of ocean carbon species in the western North Pacific using parameterization technique, J. Oceanogr., 76, 155–167, https://doi.org/10.1007/s10872-019-00532-7, 2020.

Williams, N. L., Juranek, L. W., Johnson, K. S., Feely, R. A., Riser, S. C., Talley, L. D., Russell, J. L., Sarmiento, J. L., and Wanninkhof, R.: Empirical algorithms to estimate water column pH in the Southern Ocean, Geophys. Res. Lett., 43, 3415–3422, https://doi.org/10.1002/2016GL068539, 2016.

Wolf-Gladrow, D. A., Zeebe, R. E., Klaas, C., Körtzinger, A., and Dickson, A. G.: Total alkalinity: The explicit conservative expression and its application to biogeochemical processes, Mar. Chem., 106, 287–300, https://doi.org/10.1016/j.marchem.2007.01.006, 2007.

Wood, K. R., Bond, N. A., Danielson, S. L., Overland, J. E., Salo, S. A., Stabeno, P. J., and Whitefield, J.: A decade of environmental change in the Pacific Arctic region, Prog. Oceanogr., 136, 12–31, https://doi.org/10.1016/j.pocean.2015.05.005, 2015.

Woosley, R. J.: Evaluation of the temperature dependence of dissociation constants for the marine carbon system using pH and certified reference materials, 2021.

Woosley, R. J. and Millero, F. J.: Freshening of the western Arctic negates anthropogenic carbon uptake potential, Limnol. Oceanogr., 65, 1834–1846, https://doi.org/10.1002/lno.11421, 2020.

Woosley, R. J., Millero, F. J., and Takahashi, T.: Internal consistency of the inorganic carbon system in the Arctic Ocean, Limnol. Oceanogr. Methods, 15, 887–896, https://doi.org/10.1002/lom3.10208, 2017.

https://doi.org/10.5194/egusphere-2023-1386
Preprint. Discussion started: 11 July 2023

Yamamoto-Kawai, M., McLaughlin, F. A., Carmack, E. C., Nishino, S., and Shimada, K.: Aragonite undersaturation in the Arctic Ocean: effects of ocean acidification and sea ice melt, Science, 326, 1098–1100, https://doi.org/10.1126/science.1174190, 2009.

Zeng, J., Chen, M., Zheng, M., Hu, W., and Qiu, Y.: A potential nitrogen sink discovered in the oxygenated Chukchi Shelf waters of the Arctic, Geochem. Trans., 18, 5, https://doi.org/10.1186/s12932-017-0043-2, 2017.

Tables

Table 1. Chukchi Ecosystem Observatory location and instrument sampling periods. Values in parenthesis indicate the number of measurements averaged within each measurement interval window.

			SUNA V2	HydroC CO_2	SBE16	SBE37	SeaFET	SBE63
Parameters	Latitude	Longitude	NO_3	pCO_2	CTD+	CTD	pH	O_2
2016-2017	71.5996	-161.5184	1 h	12 h (300/5min)*	1 h	-	-	-
2017-2018	71.5997	-161.5189	1 h	12 h (5/5min)	2 h	2 h	2 h (30/5min)	2h
2018-2019	71.5999	-161.5281	1 h	24 h (5/5min)	1 h	2 h*	-	2 h*
2019-2020	71.59966	-161.5275	1 h	12 h (5/5min)	2 h	-	-	-

* indicate the sensor did not return data over the whole year due to battery failure
CTD+ indicates ancillary data was available with the SBE16 file (chl-*a* fluorescence, PAR, etc)

Table 2. Evaluation of pH_{SeaFET} and pH^{est} using reference pH from nearby discrete samples (pH^{disc}_{calc}). Uncertainty, u_c, is the propagated combined standard uncertainty from *errors.m* (Orr et al., 2018). pH_{SeaFET} and pH^{est} were interpolated to the discrete timestamp.

Date	Cruise	Cast No.	Distance (km)	$pH^{disc}_{calc} \pm u_c$	Anomaly (pH^{est}-pH^{disc}_{calc})	Anomaly (pH_{SeaFET}-pH^{disc}_{calc})	Source
2017-09-10	HLY1702	127	0.52	8.0123±0.0166	-0.0450*	-0.0354	Cross et al., 2020a
2019-08-11	HLY1901	39	3.75	7.6423±0.012	0.0079*	-	Cross et al., 2021
2019-08-19	OS1901	33	0.27	7.7367±0.0145	-0.0200	-	unpublished

https://doi.org/10.5194/egusphere-2023-1386
Preprint. Discussion started: 11 July 2023

* indicates pH^{disc}_{calc} was interpolated to mooring depth							

1257

1258

https://doi.org/10.5194/egusphere-2023-1386
Preprint. Discussion started: 11 July 2023

1259 **Figures**

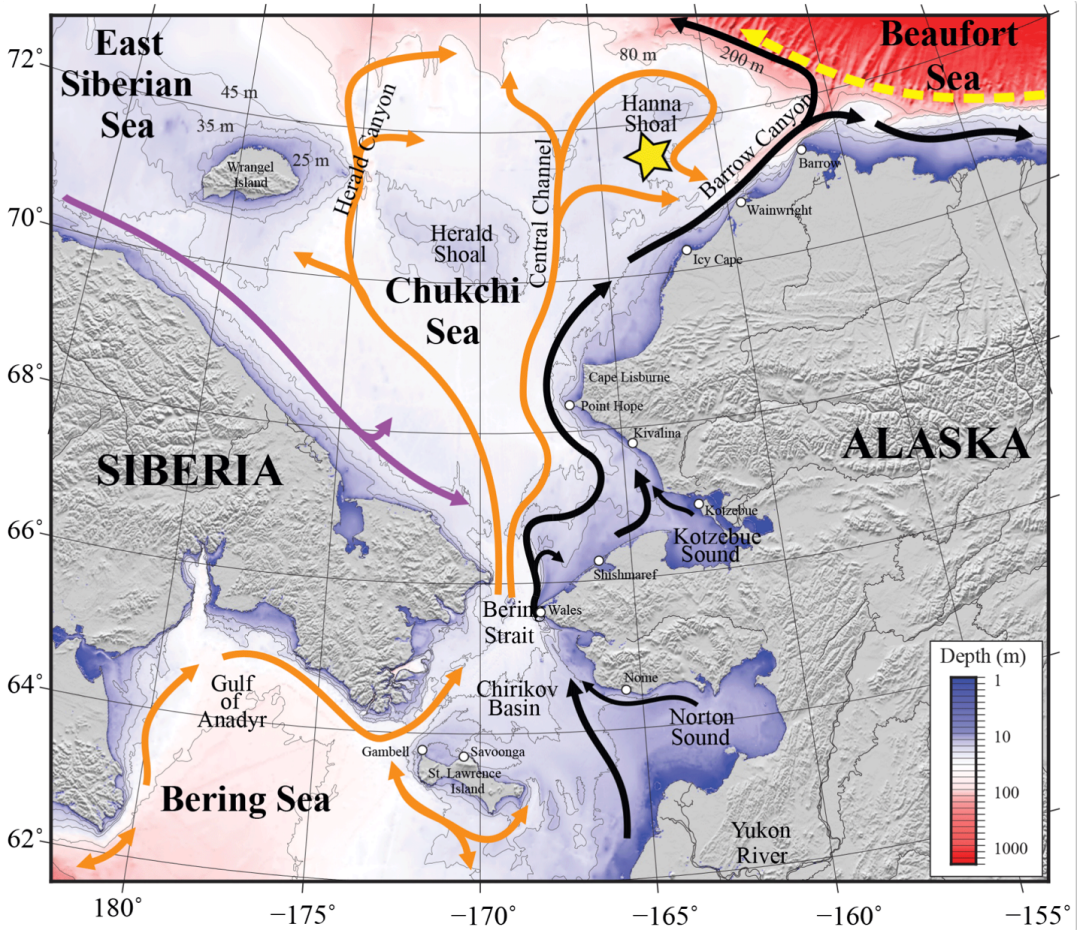

1260

1261 **Figure 1. Map of the study area.** Bathymetry of the Chukchi, northern Bering, East Siberian
1262 and eastern Beaufort seas is shown in color. The Chukchi Ecosystem Observatory (CEO) near
1263 Hanna Shoal is marked with a yellow star. General circulation patterns are shown with arrows:
1264 black – Alaskan Coastal Water and Alaskan Coastal Current, dividing into the Shelf-break Jet
1265 (right) and Chukchi Slope Current (left, Corlett and Pickart, (2017)); orange – Anadyr, Bering,
1266 and Chukchi Seawater; purple – Siberian Coastal Current; yellow – Beaufort Gyre boundary
1267 current. Figure is from (Hauri et al., 2018).

1268

https://doi.org/10.5194/egusphere-2023-1386
Preprint. Discussion started: 11 July 2023

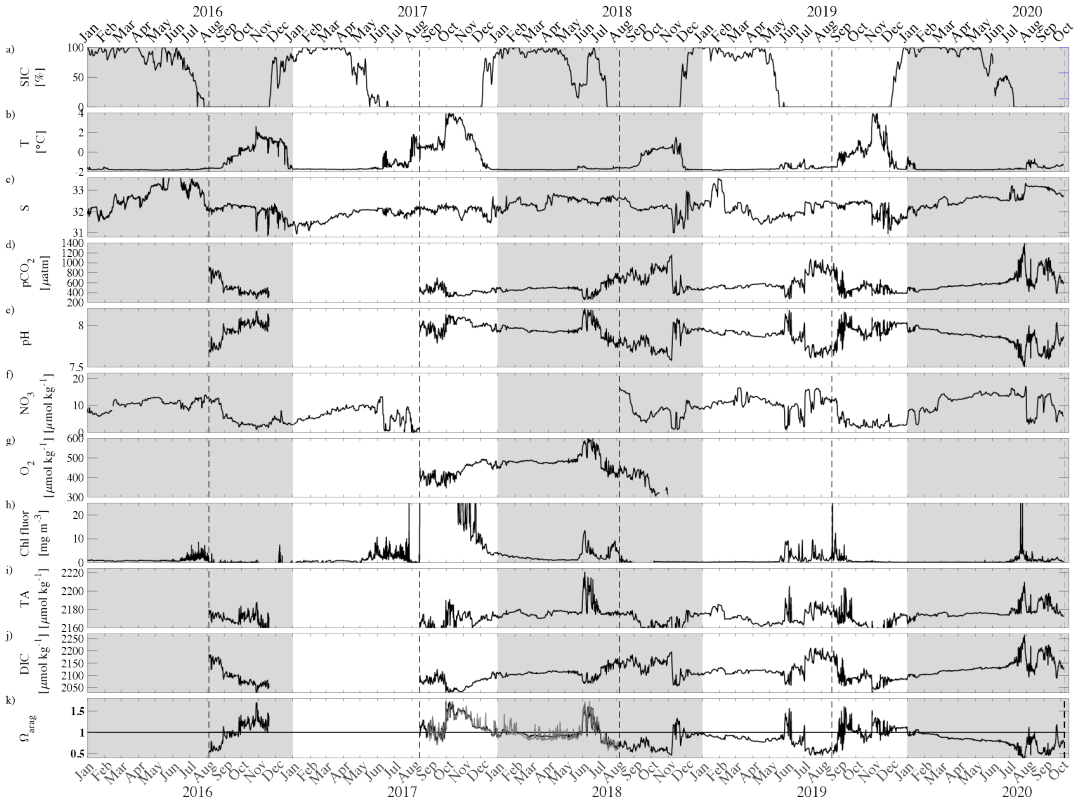

Figure 2. Chukchi Ecosystem Observatory timeseries from 2016 through 2020. Shown are a) sea ice concentration (%; DiGirolamo et al., 2022), b) temperature (°C), c) salinity, d) pCO_2 (µatm; Hauri and Irving, 2023a), e) pH (estimated in black, measured in gray; Hauri and Irving 2023b), f) NO_3 (umol kg^{-1}), g) dissolved oxygen (umol kg^{-1}), h) chlorophyll fluorescence (mg m^{-3}), i) total alkalinity (umol kg^{-1}), j) dissolved inorganic carbon (umol kg^{-1}), and k) aragonite saturation state (Ω_{arag}). Years are indicated by alternating grey and white background shading. The vertical dotted gray lines indicate the mooring turn around timing.

https://doi.org/10.5194/egusphere-2023-1386
Preprint. Discussion started: 11 July 2023

1279

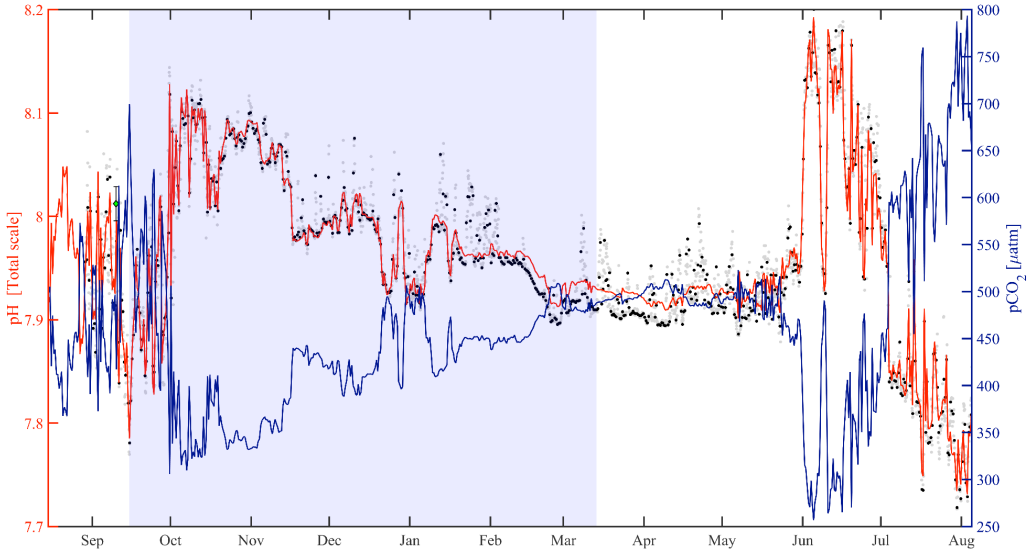

1280
1281

1282 **Figure 3**. **HydroC pCO_2 (solid blue line) and SeapHOx pH (black and gray circles)**
1283 **highlighting mirrored trend from mid-August 2017 to beginning of August 2018.** Measured
1284 pH is shown at its original resolution (2 hr, gray circles) and interpolated onto the HydroC
1285 timestamp (12 hr, black circles), and estimated pH is shown as the solid red line. The blue
1286 highlighted section shows the period over which estimated pH was trained. The green faced
1287 diamond with error bars show reference $pH^{disc}_{calc} \pm u_c$ (Cross et al., 2020a; Orr et al., 2018).

1288

https://doi.org/10.5194/egusphere-2023-1386
Preprint. Discussion started: 11 July 2023

1289

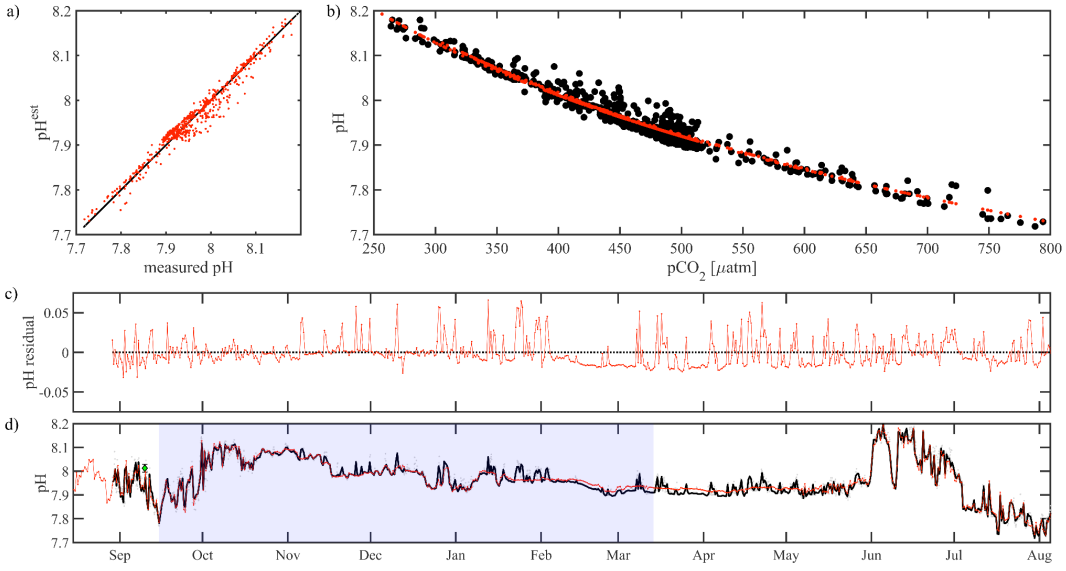

1290

1291 **Figure 4**. **Evaluation of estimated pH.** (a) measured pH vs estimated pH (pH^{est}), (b) measured
1292 pCO_2 vs pH (black) and pCO_2 vs pH^{est} (red), (c) residual pH (measured pH – pH^{est}) and (d)
1293 measured pH (black) and pH^{est} (red) vs. time. The blue highlighted section in (d) shows the
1294 period over which pH^{est} was trained (15 September - 14 March 2017) with $pH^{disc}_{calc} \pm u_c$ for
1295 reference (green faced diamond with error bar showing combined standard uncertainty; Cross et
1296 al., 2020a; Orr et al., 2018).

1297

https://doi.org/10.5194/egusphere-2023-1386
Preprint. Discussion started: 11 July 2023

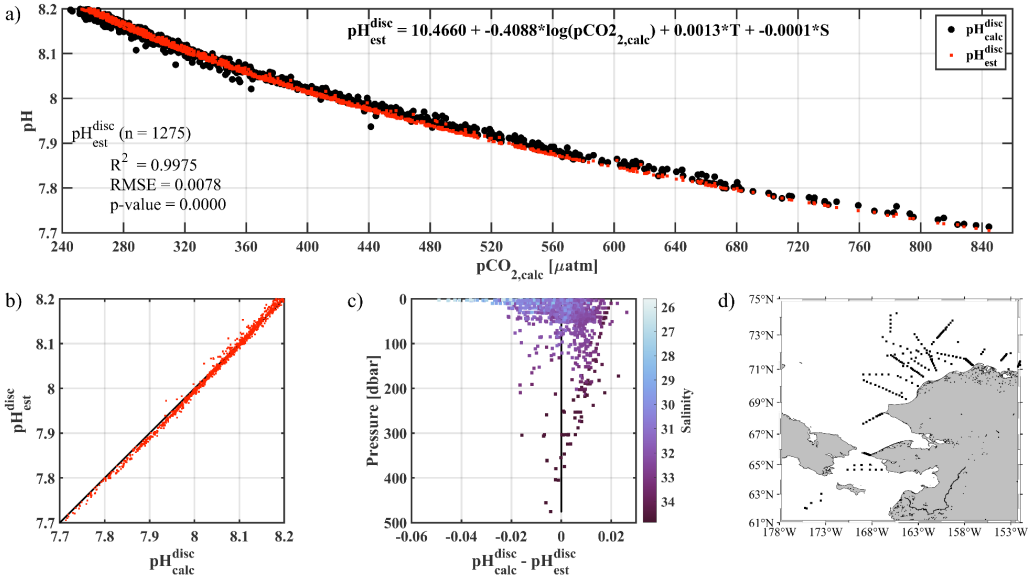

Figure 5. pH algorithm evaluation with pH from discrete samples collected in fall 2017-2020 and pH estimated using our linear regression model. (a) calculated pCO_2 (TA, DIC) vs pH (black pH^{disc}_{calc} and red pH^{disc}_{est}), (b) pH^{disc}_{calc} vs. pH^{disc}_{est}, (c) residual pH (pH^{disc}_{calc} - pH^{disc}_{est}) vs depth with color shading by salinity, and (d) map showing locations of 1275 discrete water samples used for evaluation (Monacci et al., 2022; Cross et al., 2021; 2020a; 2020b).

https://doi.org/10.5194/egusphere-2023-1386
Preprint. Discussion started: 11 July 2023

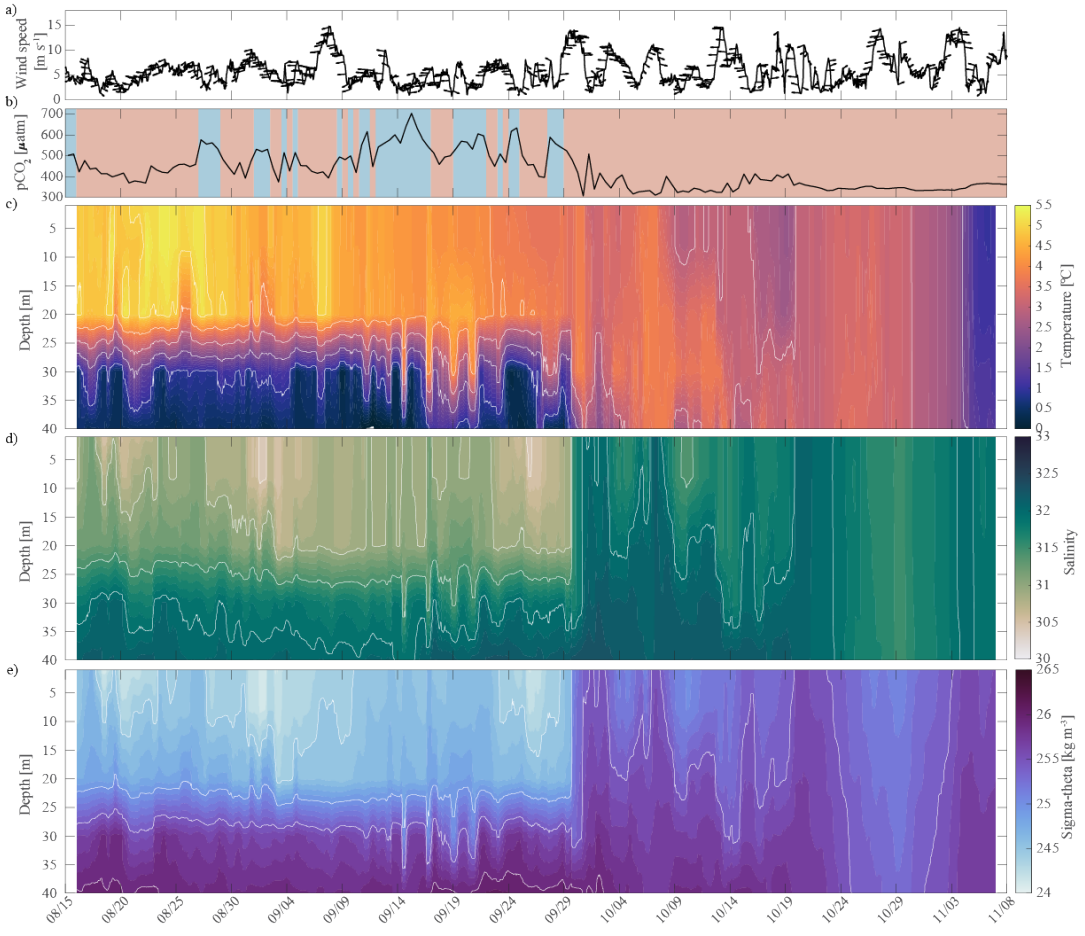

Figure 6. Water column structure from late summer 2017 to freeze up. Profiles of a) wind speed and direction (arrows pointing downwind) from the NOAA-operated Wiley Post-Will Rogers Memorial Airport, b) pCO_2 (µatm) with blue background indicating the water was undersaturated regarding aragonite ($\Omega_{arag} < 1$) and red shading indicating aragonite oversaturation ($\Omega_{arag} >= 1$), c) temperature (°C), d) salinity, and e) sigma-theta (kg m^{-3}). Temperature (c) and salinity (d) were measured at 8, 20, 30, and 40 m by the Chukchi Ecosystem Observatory freeze-up detection mooring deployed in fall 2017. Density was calculated with the TEOS-10 GSW Oceanographic Toolbox (McDougall and Baker, 2011).

https://doi.org/10.5194/egusphere-2023-1386
Preprint. Discussion started: 11 July 2023

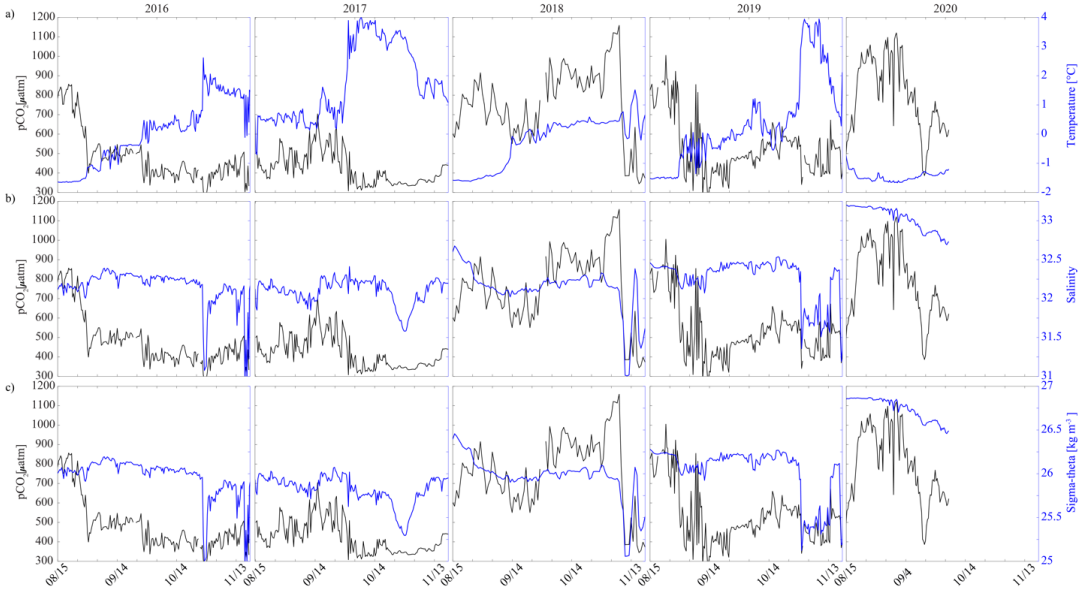

Figure 7. Impact of water column mixing on pCO_2. Timeseries of pCO_2 (black, left axis) and a) temperature (blue, right axis), b) salinity (blue, right axis), and c) density (blue, right axis) for 15 August to 1 December in 2016 -2020 measured at ~33m at the Chukchi Sea Ecosystem Observatory.

https://doi.org/10.5194/egusphere-2023-1386
Preprint. Discussion started: 11 July 2023

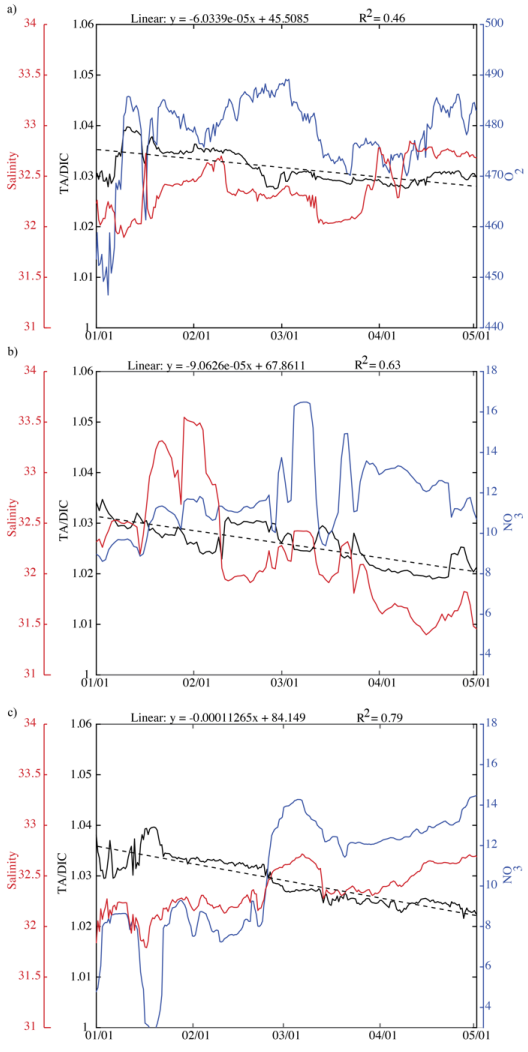

Figure 8. **Respiration under the sea ice.** Timeseries of TA/DIC ratio and salinity (left axis), and nitrate (NO_3, umol kg^{-1}) concentration (right axis) during January through April for 2018 (top), 2019 (middle) and 2020 (bottom).

https://doi.org/10.5194/egusphere-2023-1386
Preprint. Discussion started: 11 July 2023

1342

1343

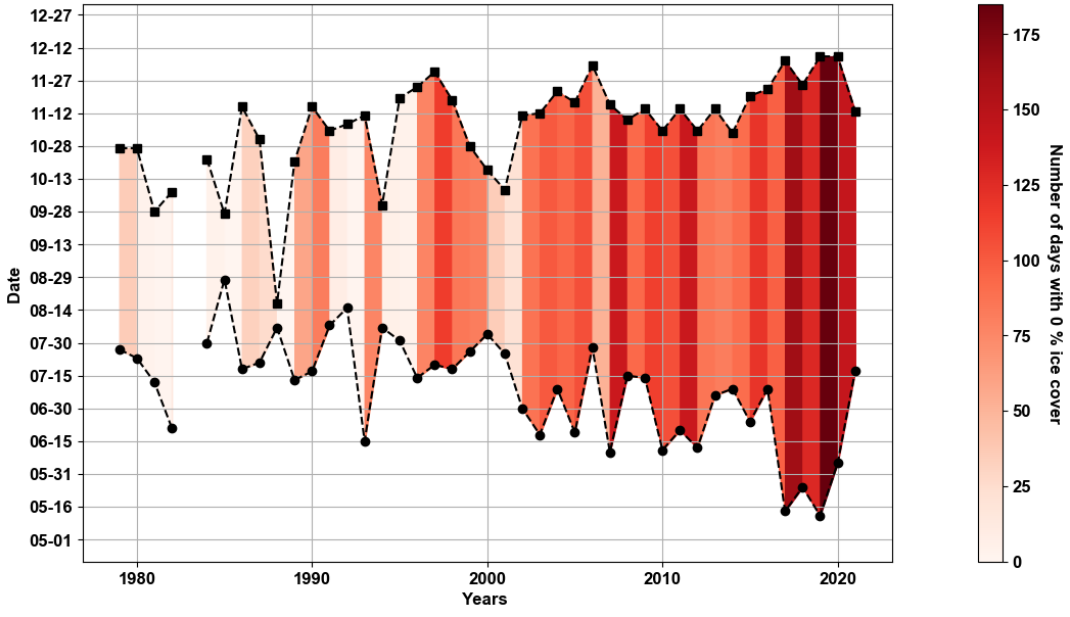

1344

1345

1346

1347 **Figure 9. Low sea ice period at the Chukchi Sea Observatory.** Timeseries of start (circle) and
1348 end (square) of low sea ice (< 51% per grid cell) period from 1982-2021. Shades of red illustrate
1349 number of days with 0 sea ice cover. The satellite sea ice cover at the observatory site was taken
1350 from the NSIDC (DiGirolamo et al., 2022).